Microstructural Characterization of Al-Ag-Cu Eutectic System

by
Mehmet Emre Çetinkaya

A Thesis Submitted to the
Graduate School of Sciences and Engineering
in Partial Fulfillment of the Requirements for
the Degree of

Master of Science
in
Mechanical Engineering

Koç University
September 2018

Koç University

Graduate School of Sciences and Engineering

This is to certify that I have examined this copy of a master's thesis by

Mehmet Emre Çetinkaya

and have found that it is complete and satisfactory in all respects,
and that any and all revisions required by the final
examining committee have been made.

Committee Members:

Melis Şerefoğlu Kaya, Ph. D. (Advisor)

Murat Sözer, Ph. D.

Derya Dışpınar, Ph. D.

Date: _____

ABSTRACT

Characterization of microstructure is vital to be able to control properties of materials. Solidification is one of the major process for the formation of microstructure. For eutectic solidification microstructures, while extensive studies were performed on binary systems, microstructure evolution in multiphase systems are still needed to be understood. Al-Cu-Ag system is a good candidate to study microstructure evolution in multiphase materials due to both being model alloy and offering a variety in microstructural features. Moreover, well-established phase diagram and thermo-physical properties make it easier to understand the dynamics of solidification. However, existence of three phases in Al-Cu-Ag system, namely (Al), Al_2Cu, Ag_2Al, orientation relationships, and anisotropic crystal/crystal interphases lead to very complex microstructures.

In this work, Al-Ag-Cu samples at the nonvariant composition are directionally solidified by highly controlled Bridgman type setup. Experiments are performed in the velocity range of 0.1 μm/s to 4.0 μm/s and at a constant thermal gradient of 15 K/mm. The thermal gradient and the purity of the alloy are sufficient to form planar S/L interface which is extremely important for the eutectic microstructure studies. The structures formed at various growth velocities are quantitatively characterized in terms of morphology and microstructure using newly-established method which involves Feret technique. In addition, phase fraction and area are measured as a function of growth length. The mostly observed pattern for the Al-Ag-Cu eutectic system is determined to be chain-like structure. Microstructural changes over the growth length is investigated and formation of paw structure and faceted structure are examined. $\lambda^2 V$ fitting on the eutectic spacing data taken from microstructures grown within the velocity range shows that the microstructure follows the Jackson & Hunt scaling law [1]. Additionally, different size samples are used to determine the effect of convection on the microstructure. As a result, three phase Al-Ag-Cu eutectic system is characterized in terms of solidification velocity, growth length and sample size.

ÖZET

Mikroyapı karakterizasyonu malzeme özelliklerini kontrol edebilmek adına önemlidir. Ötektik mikroyapılarda, biner sistemler üzerine oldukça geniş araştırmalar varken çok fazlı sistemlerde mikroyapı evriminin daha detaylı çalışılması gerekmektedir. Hem model alaşım olması hem de çeşitli mikroyapı özellikleri sunması sebebiyle Al-Cu-Ag sistemi çok fazlı sistemlerde mikroyapı evrimi çalışmak için iyi bir adaydır. Ek olarak, faz diyagramı ve termo fiziksel özelliklerinin iyi bilinmesi sebebiyle katılaşma dinamiklerini incelemeyi kolaylaştırmaktadır. Fakat Al-Ag-Cu sisteminde (Al), Al_2Cu, Ag_2Al şeklinde üç adet faz bulunması, faz oryantasyon ilişkileri ve katı/katı arayüzey anizotropisi karmaşık mikroyapıların oluşmasına sebep olmaktadır.

Bu tez kapsamında, değişkensiz ötektik kompozisyondaki Al-Ag-Cu numuneler, yüksek kontrollü Bridgman tipi deney düzeneği ile tek yönlü katılaştırılmıştır. Deneyler 0,1 μm/s ve 4,0 μm/s hız aralığında ve sabit 15 K/mm termal gradyan altında gerçekleştirilmiştir. Termal gradyan ve alaşımın yüksek saflığı, ötektik mikroyapı araştırmaları için oldukça önemli olan düzlemsel katı/sıvı arayüzeyi elde etmek için yeterlidir. Farklı büyüme hızlarında elde edilen numuneler morfoloji ve mikroyapı bakımından yeni geliştirilen Feret tekniği sayesinde kantitatif olarak karakterize edilmiştir. Ek olarak, faz oranları ve alanları büyüme uzunluğun boyunca ölçülmüştür. Al-Ag-Cu ötektik sistemi için en çok rastlanan yapı zincir benzeri olarak rapor edilmiştir. Büyüme uzunluğu ile değişen mikroyapısal farklılıklar araştırılmış, pati yapısı ve fasetli yapının oluşumu incelenmiştir. Belirli hız aralığında büyütülen mikroyapılardan elde edilen ötektik mesafe verisi, mikroyapının Jackson & Hunt kuralına uyduğunu göstermiştir [1]. Ek olarak, farklı çaptaki numuneler kullanılarak konveksiyonun mikroyapı üzerindeki etkisi anlaşılmaya çalışılmıştır. Sonuç olarak, katılaşma hızı, büyüme uzunluğu ve numune büyüklüğü etkileri test edilerek Al-Ag-Cu ötektik sisteminin çeşitli yönlerden karakterize edilmiştir.

ACKNOWLEDGEMENTS

Foremost, I would like to express my sincere gratitude to my advisor Melis Şerefoğlu Kaya for the continuous support of my research, for her patience, motivation, enthusiasm, and immense knowledge. Her guidance helped me in all the time of research and writing of this thesis.

Besides my advisor, I would like to thank the rest of my thesis committee: Dr. Murat Sözer and Dr. Derya Dışpınar since they accepted to being part of my thesis committee in their busy schedule.

I thank my fellow lab-mate Samira Mohagheghi for her support in my research. Also I thank my friends in Koc University: Göktuğ Gönel, Soheila Kharratiankhameneh, Sertaç Yazgı, Burak Tosun, Fatih Rahim for their motivational talks and close friendship during my master study.

I would like to express my appreciation to Dr. Eşref Ünsal for his visionary guidance in all aspects, people from Kuytam: Dr. Barış Yağcı, Dr. Amir Motallebzadeh, Dr. Ceren Yılmaz Akkaya and Kamil Kiraz for their patient help all the time and contribution to my tests and analyses. I also thank to Koç University staff: Türkan Eryiğit, Muzaffer Bütün, Muharrem Güler, Selim Ölçer, Ayşe Kızıltaş and Elif Tüysüz for their support and high energy.

In addition, I thank Dr. Ulrike Hecht and Dr. Stephan Rex from Access RWTH-Aachen for their support during the space experiments and for EBSD analysis.

I would like to thank my family: my parents Erol Çetinkaya and Neriman Çetinkaya, for teaching me the most valuable wealth: education as well as my cute sisters, for being my source of happiness.

Last but not least, I thank my wife Şule Esra who always supports me for any difficulty I encounter and loves me unconditionally. She is my safe harbor and the source of peace, energy and motivation.

This work is supported by the Scientific and Technological Research Council of Turkey (TUBITAK), under award No. 114M225.

TABLE OF CONTENT

ABSTRACT ii

ÖZET iii

LIST OF TABLES viii

LIST OF FIGURES ix

1. INTRODUCTION 1

1.1. Eutectic Reaction 1

1.1.1. Regular and Irregular Eutectics 3

1.1.2. Coupled Growth 5

1.1.3. Jackson-Hunt Theorem 6

1.2. Solubility of Silver and Copper in Aluminum 7

2. EXPERIMENTAL PROCEDURE 10

2.1. Sample Preparation 10

2.2. Directional Solidification Procedure 11

2.3. Thermal Gradient Measurement 13

2.4. Metallographic Preparation 16

2.5. Image Processing 18

2.6. Particle Based Measurement Technique Feret 21

3. RESULTS & DISCUSSION 24

3.1. Microstructures of Directionally Solidified Al-Ag-Cu Eutectic System 26

3.1.1. Chain-like Structure 29

3.1.2. Paw Structure 33

3.1.3. Initial Transient Microstructure 36

3.1.4. Faceted Structure 37

3.1.5. Sample Size Effect on Microstructure 45

3.1.6. Microstructural Characterization 50

3.1.7. Rainbow Structure 53

4. SUMMARY & CONCLUSION 56

5. REFERENCES 58

LIST OF TABLES

Table 1. The thermal gradient values obtained with different control parameters which are temperature of the furnace and circulating water (T_{hot} & T_{cold}), isolation height and velocity. (Two thermocouples are used for accurate measurement). 16
Table 2. Velocity and eutectic spacing, phase fraction and average particle area values measured from chain-like structures. 33
Table 3. Comparison of eutectic spacing values between chain-like and paw structures at the same growth velocity and different growth lengths. 36
Table 4. Elemental compositions obtained from ICP-MS test in atomic and weight percentages. 0 represents as cast state and 120 is the sample taken from 120 mm growth length. 42
Table 5. Eutectic spacing parameters measured in samples grown with different growth velocities and with different diameters. 50
Table 6. Measured $\lambda^2 V$ for samples with 3 and 5 mm diameters. 52

LIST OF FIGURES

Figure 1. Types of atomic solid/liquid (S/L) interface, (a) rough interface and isotropic Wulff plot corresponding to it, (b) smooth interface forming faceted structure and anisotropic Wulff plot corresponding to it. [2] 2
Figure 2. Regular and irregular eutectics: (a) regular Al-Au eutectic observed in a longitudinal section; (b) irregular Al-Si eutectic observed in a transverse section; (c) regular CBr_4-C_2Cl_6 eutectic observed during growth; (d) an irregular borneolsuccinonitrile eutectic observed during growth. The faceted borneol phase leads the growth of succinonitrile in between. [2] 4
Figure 3 (a) A typical eutectic phase diagram, (b) a schematic diagram of the coupled growth of α- and β-lamellae during directional solidification of binary eutectic system. [2] 5
Figure 4. (a) Ag-Al phase diagram, (b) Ag solubility region on Ag-Al phase diagram [35]. 8
Figure 5. (a) Al-Cu phase diagram, (b) Cu solubility region on Al-Cu phase diagram [35], [36]. ... 8
Figure 6. SEM image of directionally solidified (V = 1.2 μm/s) sample (a) Growth length is 17 mm (b) Growth length is 1 mm below quench interface. 9
Figure 7. a) Air entrapment results from Magmasoft casting simulation program b) Stainless steel mold for manufacturing of rods with 5 mm in diameter. 11
Figure 8. Schematic representation of the Bridgman unit. 13
Figure 9. Temperature vs. position graph used for thermal gradient measurement. F1, F2, and F3 are furnace, TC1 and TC2 are thermocouple temperature values. Furnace temperature: 900 ^oC, water circulation temperature: 25 ^oC, isolation height: 30 cm, velocity: 100 μm/s. 15
Figure 10. Sample obtained after longitudinal grinding and polishing (Dashed lines represent the cutting positions for cross sectional analyses). 17
Figure 11. An example of SEM image from the cross-section of directionally solidified Al-Ag-Cu at V = 1.0 μm/s. 18
Figure 12. Image processed SEM image shown in Figure 11. (Improvements on image: Noise despeckle, brightness/contrast adjustment, and Gaussian blur). 19
Figure 13. Binarized images and particles measured from the image shown in Figure 11 (a) (Al) particles converted to white and the outline of (Al) particles are shown, (b) Ag_2Al particles converted to white and outline of Ag_2Al particles are shown, (c) Al_2Cu particles converted to white and outline of Al_2Cu particles are shown. 20

Figure 14. (a) Definition of minimum and maximum Feret, (b) An example of a histogram graph where the data belongs to particles from a phase, orange curve is the Gaussian fit the data and dashed line points out the average value. 22
Figure 15. Definition of eutectic spacing, (a) An example SEM image from the cross-section of Al-Ag-Cu ternary eutectic alloy, (b) Normalized eutectic array. 23
Figure 16. Cross-sectional SEM Images from four different microstructures (a) Chain-like structure, (b) Initial transient microstructure, (c) Paw structure, (d) Faceted structure. 24
Figure 17. Directional solidification velocity vs. growth length graph. Colored bubbles represent different microstructures. Single letter shows one microstructure over the cross-section and double letter is for coexisting phases. 26
Figure 18. Longitudinal SEM image of directionally solidified (V = 1.2 μm/s) sample with 5 mm in diameter. Thermal gradient direction is shown by the white arrow. 27
Figure 19. Longitudinal and cross-sectional views of the directionally solidified Al-Ag-Cu eutectic alloy (V = 4.0 μm/s). Image is taken 1 mm below the S/L interface and the sample diameter is 5 mm. Black area: Al_2Cu, gray area: (Al) matrix and white area: Ag_2Al. 28
Figure 20. SEM image of directionally solidified (V = 1.5 μm/s) sample. Growth length is 40 mm and the diameter of the sample is 5 mm. Dashed red line shows the grain boundary and array directions in the grains are represented by yellow dashed lines. 30
Figure 21. Chain-like structure observed at 17 mm growth length. Black area is Al phase, gray area is Al_2Cu, and white area is Ag_2Al. Directionally solidified Al-Ag-Cu sample with 5 mm in diameter (V = 1.2 μm/s). 31
Figure 22. SEM images of directionally solidified samples with (a) 1.0 μm/s, (b) 1.2 μm/s, (c) 1.5 μm/s, (d) 4.0 μm/s at 250x magnification. All sample diameters are 5 mm. 32
Figure 23. (a) Eutectic spacing vs. velocity graph, (b) phase fraction (solid lines) and phase area (dashed lines) vs. velocity graph. Data is taken from Table 2. 33
Figure 24. The transformation of directionally solidified (V = 4.0 μm/s) sample along growth length. Sample diameter is 5 mm. (a) Completely chain-like structure at 40 mm growth length (b) mostly chain-like structure at 60 mm growth length (c) mostly chain-like structure at 80 mm growth length (d) completely paw structure at 100 mm growth length. Images are at the same magnification (1000x). 34
Figure 25. The transformation of directionally solidified (V = 1.5 μm/s) sample along growth length. Sample diameter is 5 mm. (a) Completely chain-like structure at 20 mm growth length (b)

Completely paw structure at 60 mm growth length. Images are at the same magnification (350x). 35
Figure 26. Initial transient microstructures of directionally solidified (V = 0.1 μm/s) sample (a) at 20 mm growth length, D = 5 mm (b) 40 mm growth length D = 1.5 mm. Black area is (Al) matrix, gray area is Al_2Cu and white area is Ag_2Al phase..... 37
Figure 27. SEM image of directionally solidified sample (V = 0.1 μm/s). Cross-section is at 60 mm growth length and sample diameter is 5 mm. Whole sample image at the center is taken with 50x magnification, bottom right and left images are taken with 500x magnification and top right image is taken with 1000x magnification. 38
Figure 28. SEM image of directionally solidified sample (V = 0.1 μm/s). Cross-section is at 80 mm growth length and sample diameter is 5 mm. Whole sample image at the center is taken with 50x magnification, bottom right and left images are taken with 500x magnification and top right image is taken with 1000x magnification. 39
Figure 29. SEM image of directionally solidified sample (V = 0.1 μm/s). Cross-section is at 100 mm growth length and sample diameter is 5 mm. Whole sample image at the center is taken with 50x magnification, bottom right and left images are taken with 250x magnification and top right image is taken with 500x magnification..... 40
Figure 30. EBSD analysis of the faceted structure (a) Faceted structure grown at V = 0.1 μm/s (b) EBSD results of faceted structure with Ag_2Al crystal orientations. 41
Figure 31. DSC thermograph of directionally solidified (V = 0.1 μm/s) sample at 120 mm growth length showing the start of solidification is at 550 ºC..... 43
Figure 32. Al-Ag-Cu ternary phase diagram. Isotherm obtained from DSC test is represented by red line and elemental results obtained from ICP test are represented by green line [38]..... 44
Figure 33. Initial transient microstructure obtained at samples with different inner diameters (a) SEM image of the whole sample directionally solidified with V = 0.1 μm/s at 40 mm growth length (b) The microstructure within the 5 mm diameter sample (c) The microstructure inside the 1.5 mm diameter sample..... 46
Figure 34. Mostly chain-like structure obtained at samples with different inner diameters (a) SEM image of the whole sample directionally solidified with V = 0.1 μm/s at 60 mm growth length (b) The microstructure within the 5 mm diameter sample (c) The microstructure inside the 1.5 mm diameter sample. 47
Figure 35. Faceted structure obtained in 5 mm diameter sample while structure is obtained in in 1.5 mm diameter sample after directional solidification at V = 0.1 μm/s and GL = 80 mm growth

length (b) The microstructure within the 5 mm diameter sample (c) The microstructure inside the 1.5 mm diameter sample. 48
Figure 36. Faceted structure obtained at samples with different inner diameters (a) SEM image of the whole sample directionally solidified with V = 0.1 μm/s at 100 mm growth length (b) The microstructure within the 5 mm diameter sample (c) The microstructure inside the 1.5 mm diameter sample. 49
Figure 37. Eutectic spacing vs. velocity graph in logarithmic scale for 5 mm diameter samples. Fitting is applied by using $\lambda^2 V$ equation and error bars are calculated using standard deviation with 68%..... 51
Figure 38. Eutectic spacing vs. velocity graph in logarithmic scale for 3 mm diameter samples. Fitting is applied by using $\lambda^2 V$ equation and error bars are calculated using standard deviation with 68%..... 52
Figure 39. Rainbow structure observed in directionally solidified (V = 0.1 μm/s) sample at 20 mm growth length. Sample diameter is 5 mm. 54
Figure 40. Rainbow structure observed in directionally solidified (V = 1.5 μm/s) sample at 80 mm growth length. Sample diameter is 3 mm. 55

NOMENCLATURE

ΔS_f^m	Molar entropy difference between solid and liquid
S_l^m	Molar entropy of liquid
S_s^m	Molar entropy of solid
R	Ideal gas constant
$\triangle$T	Undercooling
Δx	Position difference
K_c, K_r	Growth constants for eutectic
V	Growth velocity
λ	Eutectic spacing
λ_{JH}	Jackson-Hunt eutectic spacing
G	Thermal gradient
T_E	Eutectic temperature
C_E	Eutectic composition
D	Diffusion coefficient
k	Partition coefficient
Z	Distance to reach steady state
F	Furnace temperature
TC	Thermocouple temperature

1. INTRODUCTION

Development of civilization started thousands of years ago and human beings discovered how to use variety of materials. Their usage started for purposes such as protection, hunting, shelter, etc. and have continued to increase until today in new technologies such as lightweight aircrafts, high temperature resistant turbine blades, energy producing solar panels, and additively manufactured innovative materials. In Stone Age, shell, clay, bone and fiber were some of the materials used for the basic needs of human beings. Only copper and lead were two metals used in this age at specific areas due to their high shape-ability. However, this advantage became a disadvantage by inhibiting further usage of it for different applications. Therefore, human beings recognized to need for harder materials production. After discovery of smelting of the metal, Tin is added to Copper to produce bronze, which is the start of Bronze Age. As a result, the harder materials was shaped easily and importance of melting is understood so that history of solidification started.

Today, almost all metals used in daily life are subjected to solidification for either extraction or shaping purposes. Since all properties including mechanical, thermal, optical depend on microstructure, intensive studies focus on the microstructure. The control on the solidification process provides control on the microstructure which depends on parameters such as chemical composition, material's thermal and physical properties, solidification rate, crystallographic orientation relationships and so on. Depending on these parameters, the microstructures obtained during solidification reaction vary from dendritic, cellular to eutectic.

1.1. Eutectic Reaction

There are many possible reactions for producing metals in different shapes and properties but the most understood and easy reaction is eutectic. In this reaction, one homogenous liquid phase transforms to two or more solid phases at a specific temperature, namely, eutectic temperature. The first advantage of eutectic alloy is having a reaction temperature even lower than that pure components. Second advantage is that reaction takes place at one specific point without passing through a freezing range called "mushy zone". These two properties make eutectic alloys very suitable candidates for some processes involving casting, welding, soldering. Therefore, using eutectic alloys, one spend less energy for melting, achieves good fluidity during flow and

castability. In addition, the eutectic microstructure has a micro-composite structure that shows favorable effect on the material properties.

Since the system is not at the lowest Gibbs free energy, the thermal and solute gradients departure from equilibrium. However, at the interface, equilibrium holds and phase diagram is useful for eutectic reaction. These thermodynamic rules are affected from kinetics. There are three deviation sources which are the attachment kinetics affected by molar entropy of fusion, the surface energy of curvature and the trapping of solute elements [2]. Atom transportation from undercooled liquid to solid by atomic attachment is required. This nanoscale phenomena can occur in two ways: attachment to the atomically smooth interfaces and atomically rough interfaces (Figure 1).

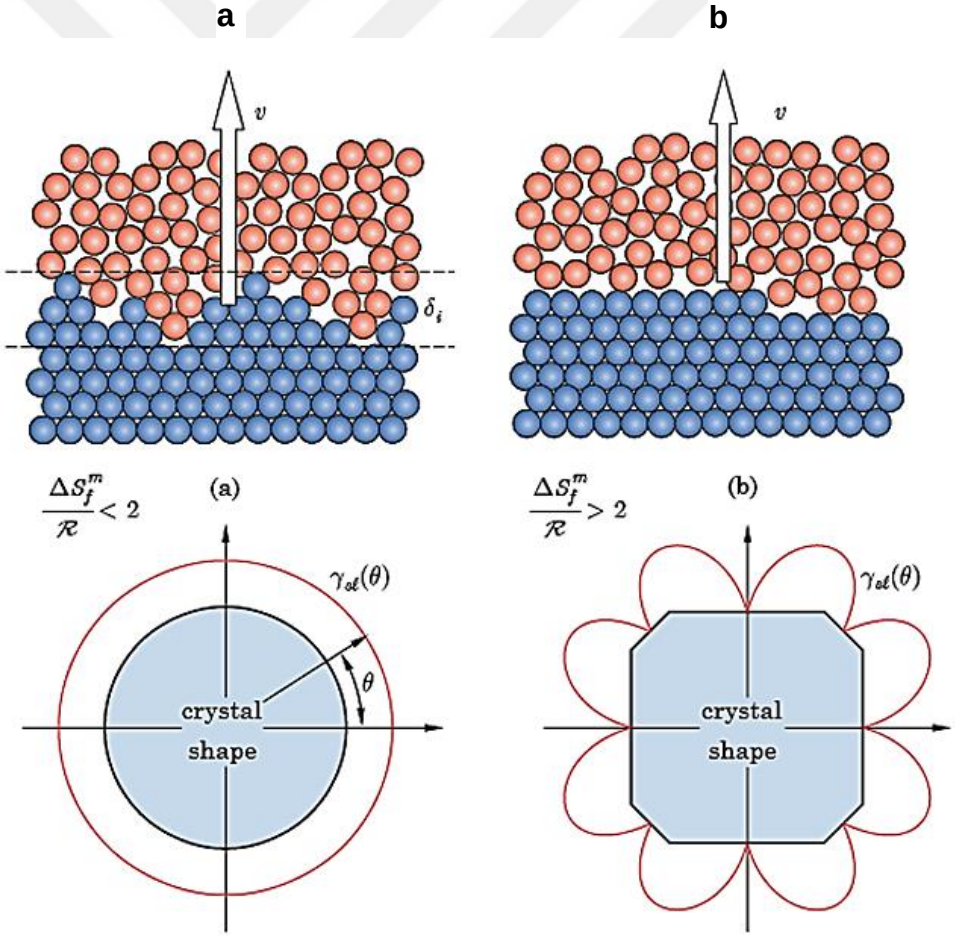

Figure 1. Types of atomic solid/liquid (S/L) interface, (a) rough interface and isotropic Wulff plot corresponding to it, (b) smooth interface forming faceted structure and anisotropic Wulff plot corresponding to it. [2]

1.1.1. Regular and Irregular Eutectics

In regular eutectics, slight difference between liquid and solid structure makes random atom attachment possible. The molar entropy of fusion must be low to maintain this relation so that S/L interfacial energy is isotropic. This difference is indicated in equation (1):

$$\Delta S_f^m = S_l^m - S_s^m < 2R \qquad (1)$$

Where ΔS_f^m is the molar entropy of fusion, S_l^m is the entropy of liquid, S_s^m is the entropy of solid and R is the ideal gas constant. Corresponding Wulff plot of S/L interface of regular eutectic has a circular shape (Figure 1a). Atoms can attach randomly and solid growth takes place orientation independent. Therefore, triple junctions can be maintained in every direction and phases can grow in the induced thermal gradient direction. In Figure 2a, Figure 2c, longitudinal views of two examples of regular eutectics, namely Al-Au and CBr_4 C_2Cl_6 binary alloys are seen. There exist a regular arrangement of the phases in the direction of induced thermal gradient.

As oppose to regular eutectics, in irregular eutectics, the liquid structure differs very much from the solid, which causes smooth S/L interface at the atomic scale. This difference is shown by equation (2):

$$\Delta S_f^m = S_l^m - S_s^m > 2R \qquad (2)$$

Therefore, smooth atomic arrangement in the solid prevents random atom attachment. Anisotropic S/L interfacial energy causes cusps in the Wulff plot of S/L interface and growth take place at the low energy orientations (Figure 1b). That is, atoms attach to the solid by following different plane orientations and crystal grows in different directions. As a result, irregular eutectic morphologies form by growth of faceted structures (Figure 2b, Figure 2d).

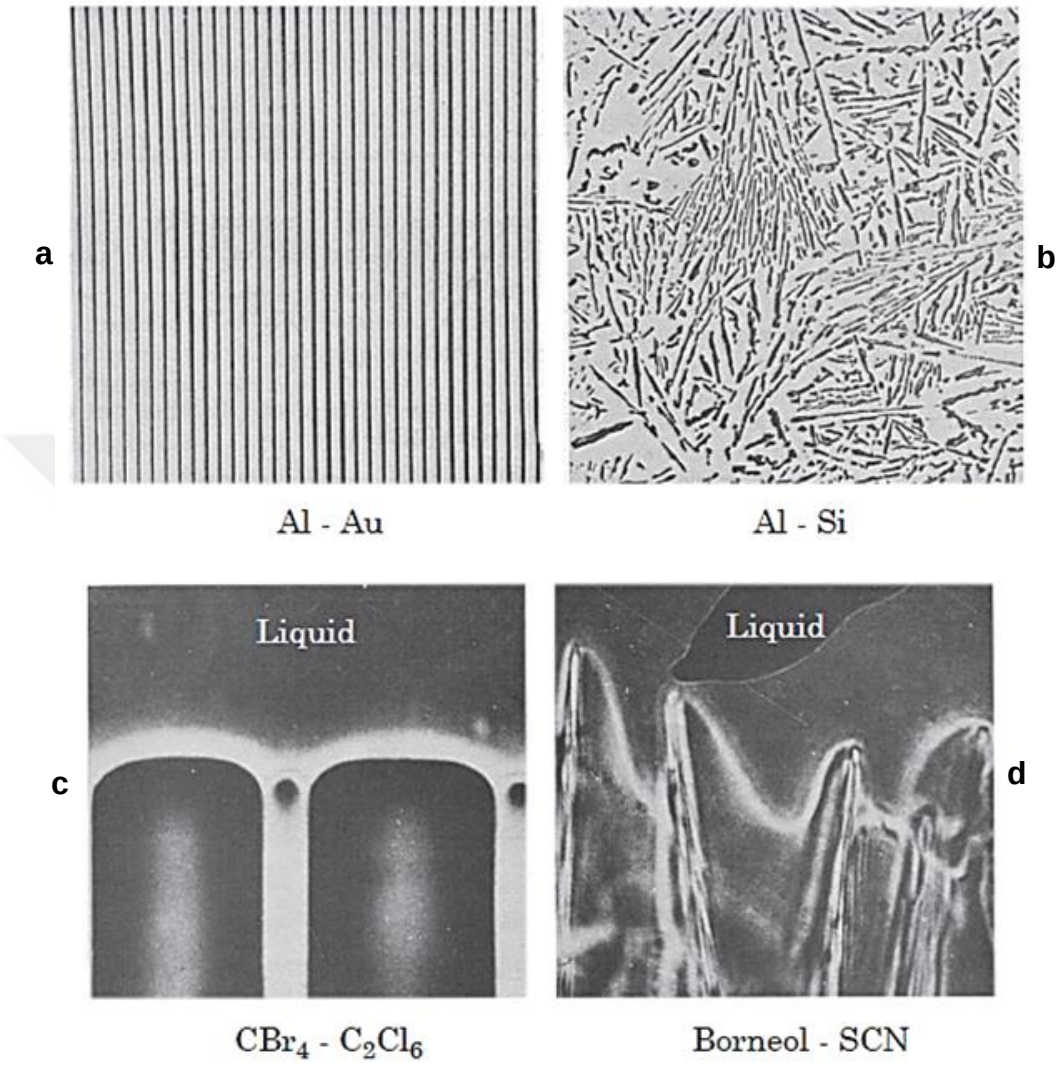

Figure 2. Regular and irregular eutectics: (a) regular Al-Au eutectic observed in a longitudinal section; (b) irregular Al-Si eutectic observed in a transverse section; (c) regular CBr_4-C_2Cl_6 eutectic observed during growth; (d) an irregular borneolsuccinonitrile eutectic observed during growth. The faceted borneol phase leads the growth of succinonitrile in between. [2]

1.1.2. Coupled Growth

Eutectic microstructure which is composed of α and β phases in a binary system forms by exchange of atoms simultaneously (Figure 3). As the example of homogenous nucleation which is more difficult than heterogeneous nucleation, separately growing phases is kinetically forbidden while mutual growth is favorable. This side by side growth mechanism is called coupled growth. This mechanism decreases the diffusion distance of atoms compared to individual growth of the eutectic phases.

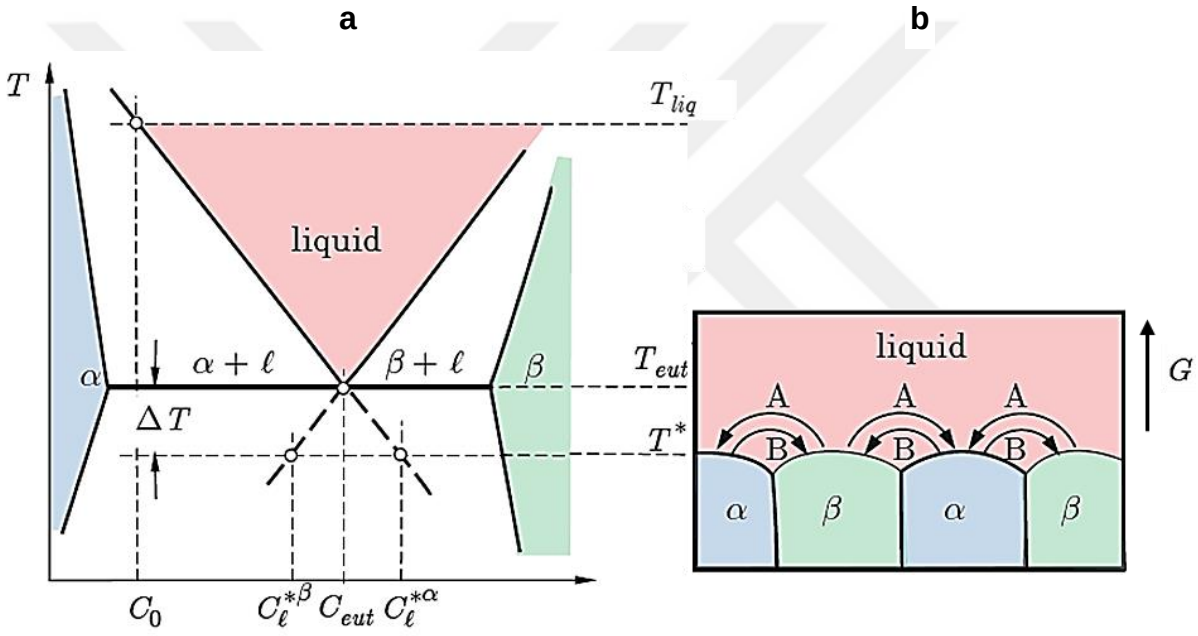

Figure 3 (a) A typical eutectic phase diagram, (b) a schematic diagram of the coupled growth of α- and β-lamellae during directional solidification of binary eutectic system. [2]

Binary eutectic systems composed of alteration of two phases in the form or rods or lamellar morphology. There have been many research conducted on different binary eutectic systems in order to understand the mechanism, microstructure and features of binary system [1, 3-12]. The most complete theory was proposed by Jackson and Hunt in 1966 [1]. According to the theory, eutectic spacing of alternating two phases is specified by two factors, curvature between solid and liquid as well as diffusion distance of the phases.

1.1.3. Jackson-Hunt Theorem

According to the theory, the undercooling necessary for coupled growth is defined by two factors which are diffusion and capillarity. To provide the shortest diffusion length for A atoms to reach to α phase and B atoms to β phase, the eutectic spacing tends to decrease. On the other hand, undercooling contributed to capillarity favors larger eutectic spacing to decrease the curvature of S/L interface. The undercooling necessary eutectic growth is clarified by Jackson-Hunt formula in equation (3):

$$\Delta T = K_r \lambda V + \frac{K_c}{\lambda} \quad (3)$$

Where ΔT is the temperature difference between eutectic temperature and S/L interface temperature ($T_{interface}<T_{eutectic}$), $K_r \lambda V$ is the average diffusion undercooling and $\frac{K_c}{\lambda}$ is the curvature undercooling. In addition, λ, V, K_r and K_c represent eutectic spacing, growth velocity, Jackson-Hunt constants respectively. By taking the derivative of equation (3) and equalizing it to 0, eutectic spacing at minimum undercooling can be calculated by the following equation:

$$\lambda_{JH}^2 V = \frac{K_c}{K_r} \quad (4)$$

According to equation (4), for the minimum undercooling, $\lambda^2 V$ is material constant and there is inversely proportional relationship between eutectic spacing and velocity.

Researchers have been studying binary eutectic systems for decades but many engineering metals are composed of three or more components and there are still a lot of unknowns for these complicated systems. This complexity comes from both having more solid/solid interphase properties and possibility of forming different arrangements in the microstructure such as ABC, ABAC, brick-like, lamella on a matrix, rod on a matrix. Eutectic spacing arrangement and morphologies has been investigated by using organic and low melting point metals at constant velocity and velocity jump experiments [13], [14], [15], [16]. In these experiments, thin samples

were used, in order to limit complexity coming from the freedom in 3D [17], [18], [19], [20]. In addition, the effect of interphase boundary anisotropy on microstructures and formation of anisotropic grains were investigated by rotating directional solidification method on In-Bi-Sn alloy [21].

One of the suitable ternary systems to study the microstructure formation an evolution during directional solidification is Al-Ag-Cu system. This is due to having nonvariant eutectic point occurring at relatively low melting point. In addition, the three phases formed during eutectic reaction have nonfaceted S/L interface. For Al-Ag-Cu system, Mccartney et al. has observed chain-like structure for the first time by using scanning electron microscope [22]. Univariant solidification structures were examined for several reasons: microstructural investigation, eutectic spacing measurement, crystallographic orientation relationship and S/L interface transformation from planar to cellular [23], [24], [25], [26], [27]. For invariant solidification, different microstructures such as H-structure, half lamella structure and irregular structure were reported with several defects from the ternary eutectic system [28], [29]. Formation of these microstructures were simulated by using phase-field method [30], [31], [32]. Although this structure is complex compared to microstructures formed in binary systems, Jackson-Hunt eutectic spacing (λ_{JH}) calculation is extended and two eutectic spacing designated [22]. According to this extension, by evaluating some material properties such as liquidus, slope of Al-Ag_2Al-Al_2Cu, diffusion and solubility limits of atoms and Gibbs-Thompson constant, λ^2V of the ternary system is theoretically and experimentally calculated [33]. Eutectic spacing, microstructural features and morphology has been characterized mathematically by using some tools such as shape factor, specific surface area, intercept method and radial distribution function [28], [34].

1.2. Solubility of Silver and Copper in Aluminum

Silver and copper have the highest solubility in aluminum phase at eutectic temperatures as it can be seen from binary phase diagrams (Figure 4 and Figure 5). If the solvus lines are considered, solubility of Ag and Cu dramatically decreases in Ag-Al and Al-Cu phase diagrams respectively. After solidification, since the solid is at high temperature, Ag is solved in (Al) matrix and forms solid solution with high concentration of Ag. However, as the temperature decreases, solubility decreases and Ag elements inside (Al) matrix phase diffuses into preformed Ag_2Al phase which causes enlargement in the phase. In addition, precipitates of Ag_2Al phase can form if the energy is sufficient for the diffusion in the solid, which is very commonly used process in industry as known as precipitation hardening of Al alloys.

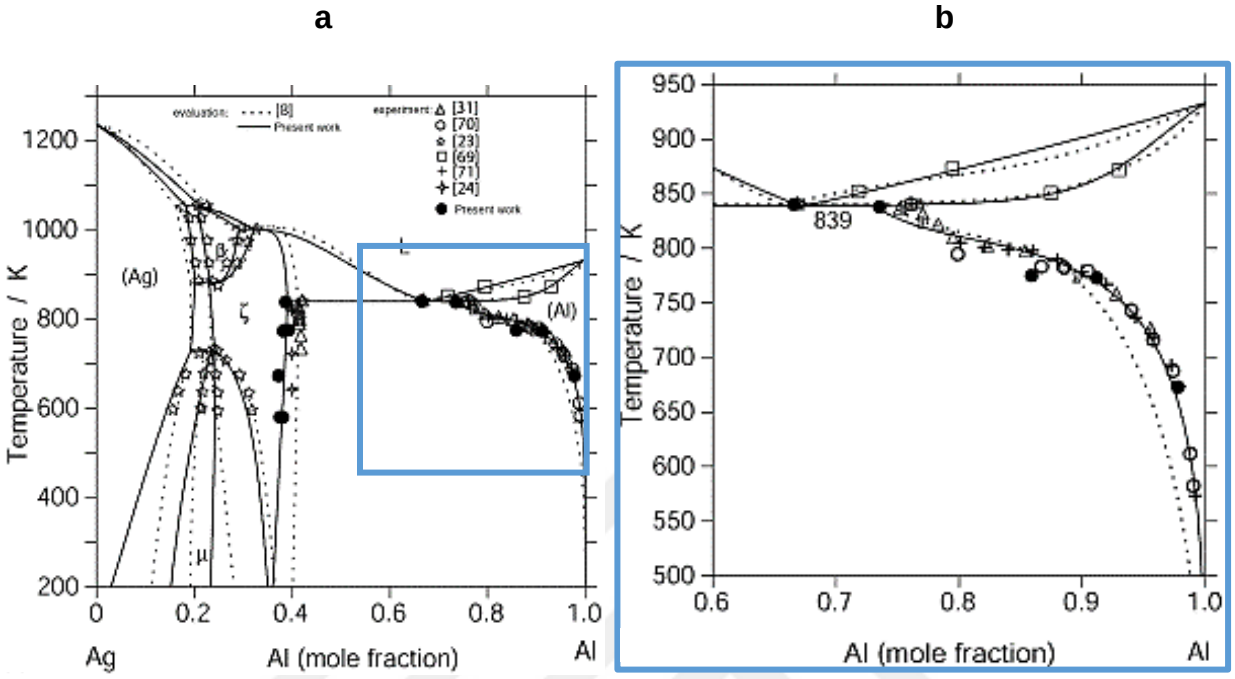

Figure 4. (a) Ag-Al phase diagram, (b) Ag solubility region on Ag-Al phase diagram [35].

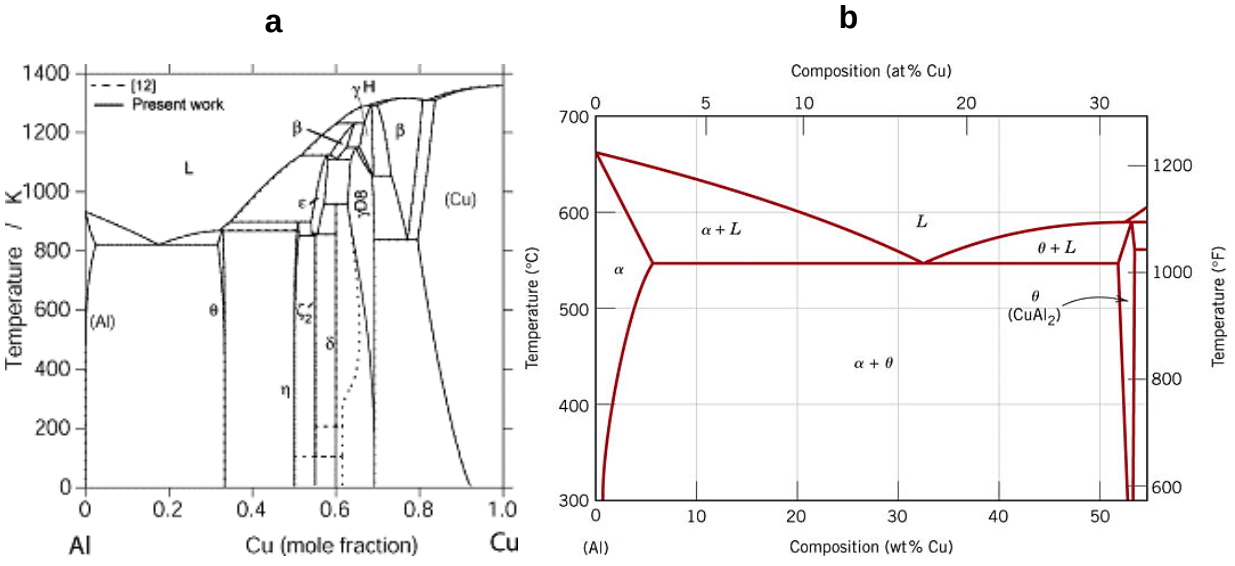

Figure 5. (a) Al-Cu phase diagram, (b) Cu solubility region on Al-Cu phase diagram [35], [36].

Quenching is essential for the investigation of solidification microstructure which is not affected by the post solidification reactions. The SEM image of directionally solidified (V = 1.2 μm/s) sample at 1 mm away from quench end is presented in Figure 6b. Unlike the microstructure obtained at 17 mm growth length Figure 6a, black area belongs to Al_2Cu and gray area belongs to (Al) matrix. The reason for that is high Ag concentration inside (Al) matrix phase due entrapment after quench. Ag is seen white under secondary electron detector so that black Al phase is converted to gray due to high Ag concentration. During directional solidification, Ag has the energy to diffuse into preformed Ag_2Al phase and enlarges this phase which is named as dog-bone structure.

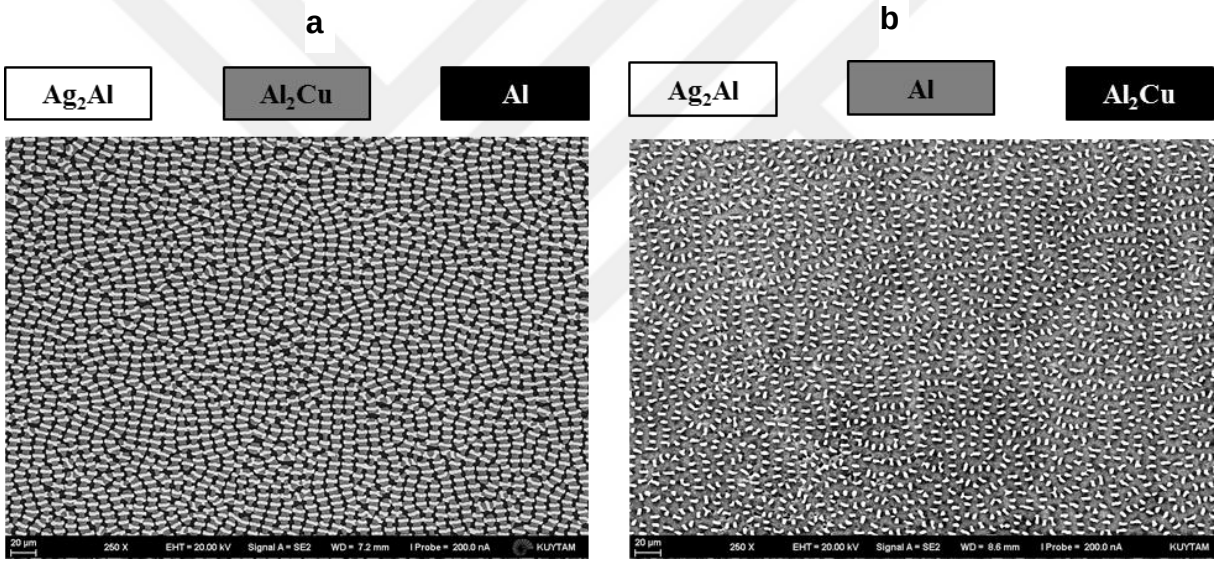

Figure 6. SEM image of directionally solidified (V = 1.2 μm/s) sample (a) Growth length is 17 mm (b) Growth length is 1 mm below quench interface.

2. EXPERIMENTAL PROCEDURE

Bridgman technique is employed to directionally solidify samples with invariant eutectic composition. Al-Ag-Cu ternary system, which has a well-known phase diagram is chosen for investigation of directionally solidified three phase eutectic system. The composition of alloy is Al – 18.1 Ag – 12.8 Cu at.% and it has a eutectic reaction at 501 ^{o}C. This eutectic reaction results in the formation of (Al) matrix, Ag_2Al and Al_2Cu intermetallic phases.

In the following sections, details of sample preparation for experiments, directional solidification procedure, gradient measurements, sample preparation for analysis, image processing and measurement techniques will be explained.

2.1. Sample Preparation

Alloy of eutectic composition is prepared with high purity (99.999%) elements. The alloy is casted into molds with different diameter channels to shape them for directional solidification experiments. The mold is designed using Magmasoft casting simulations which predetermine the porosities, air entrapment, temperature, and velocity distributions during filling and after solidification. Among the 13 designs with different rod angles, runner and gating system, the one presented in Figure 7a is selected due to the lowest air entrapment. Air entrapment should be avoided because it may result in oxidation at high temperature and impurities in directional solidification microstructures. Vertical alignment of runner and gating system is chosen in order to compensate the shrinkage that occurs during solidification. In addition, there are vertical and horizontal air escape channels with 0.2 mm depth on the inner surface of it to let the air get out of the mold. According to the selected design, the stainless steel mold shown in Figure 7b is manufactured. Boron Nitride coating is used in order to prevent sticking of the molten alloy to the walls. The mold is composed of two symmetric parts and molten alloy is poured into the cavity of the mold after closing these parts face to face. Four rods which are 5 mm or 3 mm in diameter and 200 mm in length can be produced in one casting.

a b

Figure 7. a) Air entrapment results from Magmasoft casting simulation program b) Stainless steel mold for manufacturing of rods with 5 mm in diameter.

Alumina crucible coated with Boron Nitride is filled with the alloy and placed into an electric furnace and the furnace is heated to 700 ^{o}C. Homogenization takes place after waiting for 30 minutes at this temperature and then the alloy is poured into the preheated mold. Preheating is essential for preventing misrun of the alloy during casting. The rods are cut from the connection points to the gating system. Boron Nitride residues on the rods are removed by using acetone and sample become ready for directional solidification experiments.

2.2. Directional Solidification Procedure

One rod is placed at the bottom of an alumina tube which is used as the sample holder. The rod is placed at the very bottom of the tube since any left air under the sample may form bubble during directional solidification and destroy microstructure evolution. Then, this tube is placed in the Bridgman Unit (Figure 8) for directional solidification. Bridgman Unit is composed of three main parts; heating zone, cooling zone, and motor. While the heating & cooling zone adjust the

temperature gradient; the motor moves the gradient along the sample. Firstly, the sample is heated by a tube furnace which is capable of reaching up to 1500 ^{o}C. In order to provide a specific temperature gradient, furnace is heated to 900 ^{o}C for Al-Ag-Cu samples. Secondly, cooling zone is composed of an inner conductive liquid metal and an outer water circulation channel. While the inner side provides the fastest cooling rate possible for the sample holder, the water channel keeps the temperature constant at 25 ^{o}C. The liquid metal is prepared with high purity Ga-In-Sn (Ga - 21.5 In – 16 Sn wt.%) at eutectic composition. The melting temperature of the liquid metal is 10.7 ^{o}C. The isolation separating hot and cold zones is chosen to have a height of 30 mm so that the thermal gradient is 15 K/mm at the eutectic temperature of Al-Ag-Cu alloy. It is designed to provide stationary sample holder to eliminate vibrations. Therefore, hot and cold zones move unidirectionally around the sample. A motor with a velocity range of 0.1 μm/s to 60000 μm/s provides unidirectional motion to the Bridgman Unit. While low velocities are suitable for directional solidification, higher velocities are used for quenching. The sample holder is connected to vacuum-argon line which is used to eliminate any oxidation reaction that may happen on the alloy easily at high temperatures. A summary of the directional solidification procedure is presented below:

1. Sample is placed at the bottom of the sample holder and the sample holder is fixed tightly to Bridgman Unit.
2. Air inside the sample holder is drained by vacuum and it is filled with inert gas (Argon).
3. Water circulation at 25 ^{o}C is started and the furnace is heated to 900 ^{o}C.
4. After stabilization of the S/L interface, motor motion at constant velocity is started.
5. If necessary velocity jumps are employed to investigate the influence of the velocity variations on the pattern formation.
6. Directionally solidified sample is quenched.
7. When the furnace cooled down, the sample is taken out for the metallographic preparation.

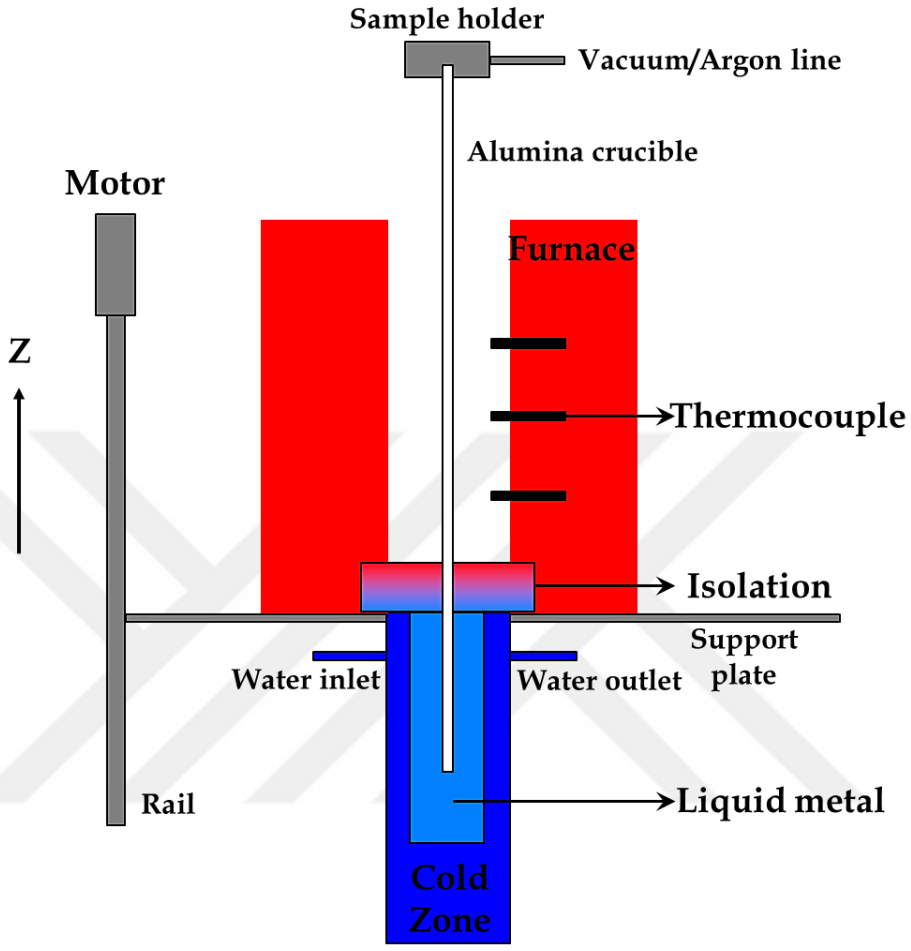

Figure 8. Schematic representation of the Bridgman unit.

2.3. Thermal Gradient Measurement

Cooling rate is the most important parameter affecting microstructure. Since cooling rate is the product of thermal gradient and solidification velocity, the maximum and the minimum thermal gradient values of the setup are measured. In our setup, cooling rate can be controlled by changing both velocity and the thermal gradient independently. Another importance of thermal gradient is that S/L interface can be planar if and only if gradient is sufficiently high in alloys. In order to investigate eutectic structures, the alloy must solidify with planar S/L interphase.

EXPERIMENTAL PROCEDURE

There are three control parameters for obtaining different thermal gradients:

1. Furnace temperature
2. Water temperature in circulator
3. Isolation material and its height

Increasing the temperature difference between cold and hot zone and decreasing the isolation height can provide higher thermal gradient values. For these tests, two K type thermocouples are placed into graphite rods for accurate measurements. The height difference between these two thermocouples is set as 10 mm.

The unit is moved directionally at a constant velocity and the isolation height which is the separator of cold and hot zone as well as furnace temperature are changed one at a time. The position value are obtained from the encoder of the motor and temperature values are obtained from thermocouples so that temperature vs. position graph is drawn. In Figure 9, the temperatures obtained from furnace thermocouples are represented as F1, F2, and F3 while TC1 and TC2 are the temperature values obtained from thermocouples inside the graphite sample.

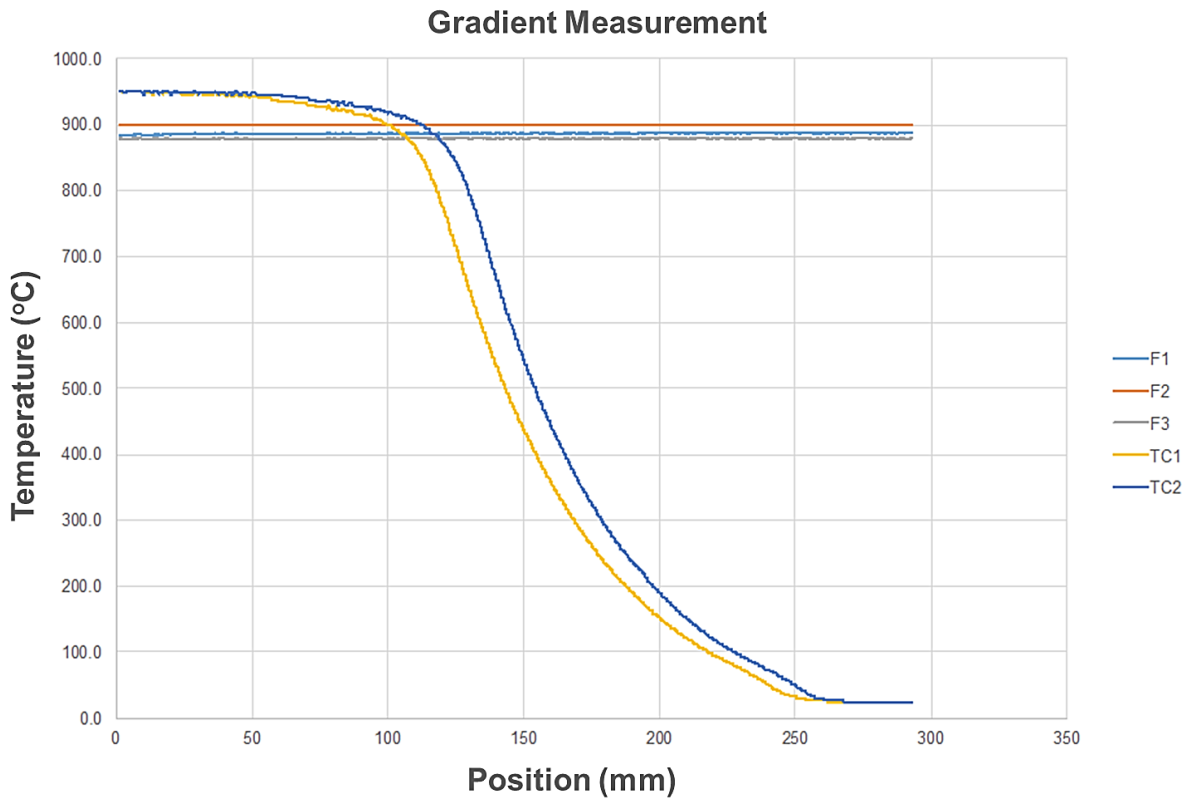

Figure 9. Temperature vs. position graph used for thermal gradient measurement. F1, F2, and F3 are furnace, TC1 and TC2 are thermocouple temperature values. Furnace temperature: 900 °C, water circulation temperature: 25 °C, isolation height: 30 cm, velocity: 100 μm/s.

The temperature gradient that is critical for microstructure evolution is the one at the S/L interface. Therefore, it is measured with a linear fit of measured temperature data around the eutectic temperature of the alloy which is at 501 °C.

In order to estimate the limits of the unit in terms of thermal gradient, different temperature and isolation height configurations are tested. In addition, effect of velocity is considered so that tests are conducted with different velocities while temperature and isolation height kept constant. Minimum and maximum thermal gradient values are determined as 9.41 and 28.30 K/mm. All configurations and thermal gradient values are presented in Table 1. The gradient used in the directional solidification experiments is shown in bold.

Table 1. The thermal gradient values obtained with different control parameters which are temperature of the furnace and circulating water (T_{hot} & T_{cold}), isolation height and velocity. (Two thermocouples are used for accurate measurement).

T_{hot} (^{0}C)	T_{cold} (^{0}C)	Velocity (μm/s)	Isolation Height (mm)	Temperature Range (^{0}C)	Gradient from TC1 (K/mm)	Gradient from TC2 (K/mm)
900	25	20	115	400 - 600	9.79	10.05
900	**25**	**100**	**30**	**400 - 600**	**14.93**	**15.00**
1200	25	100	20	450 - 650	23.49	24.93
1200	25	100	15	450 - 650	26.53	28.3
1200	25	10	15	450 - 650	21.53	23.47
1200	25	100	30	450 - 650	18.09	18.55
1200	25	10	20	450 - 650	16.76	18.33
1200	25	1	20	450 - 650	17.18	17.79
1200	25	1	15	450 - 650	17.51	18.19
1200	25	1	30	450 - 650	13.92	15.15
900	25	1	30	450 - 650	10.67	11.84
900	25	1	20	450 - 650	9.41	10.37
900	25	1	15	450 - 650	9.42	10.45

2.4. Metallographic Preparation

After directional solidification, the alumina tube is broken and the sample is taken out for microstructural investigation. While grinding eliminates impurities on the surface of the alloy, polishing is vital for elimination of all scratches. Phases of Al-Ag-Cu eutectic system does not require etching for both optical and electron microscope analyses.

Firstly, longitudinal grinding and polishing are completed. Longitudinal examination is necessary to find the positions of initiation of directional solidification, and quench interface. Abrasive paper with grit size 120 is placed on the turning table and grinding is accomplished by holding the sample on the abrasive paper until obtaining around 0.5 mm depth from the sample.

Then, abrasive papers with grit size 400, 800, 1200, and 2500 are used respectively by changing the direction of the sample 90º each time. Similarly, a cloth is placed to the turning table and paste that contains 0.3 μm size alumina is sprayed on top of the cloth. As a result, scratches are eliminated and mirror-like surface is obtained by holding the sample at different directions. The prepared sample (Figure 10) is examined under optical microscope to mark the initiation of directional solidification and quench interface positions.

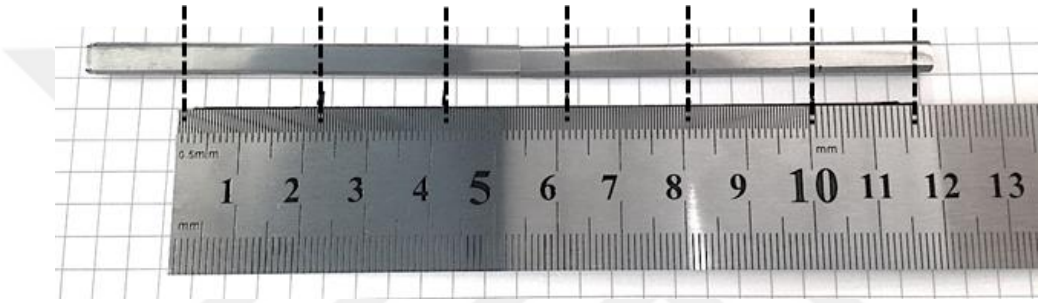

Figure 10. Sample obtained after longitudinal grinding and polishing (Dashed lines represent the cutting positions for cross sectional analyses).

Secondly, for the cross sectional examination, the sample is cut from specific growth lengths as shown in Figure 10 by using Leica TXP EM. This surface preparation device provides 0.5 mm accuracy for milling, sawing, grinding, and polishing operations so the depth of cutting and grinding can be monitored. The surface is grinded by abrasive papers with 9, 2, and 0.5 μm particle size respectively in order to eliminate scratches formed during cutting. Then, the same polishing procedure of the longitudinal polishing is applied to obtain mirror-like surface. Afterwards, microstructures at these surfaces can be analyzed under Scanning Electron Microscope (SEM).

2.5. Image Processing

Images taken from scanning electron microscope are characterized in terms of particle area, particle perimeter, particle caliper length and total area fractions. In order to measure particles objectively, image processing software is required. Image processing and particle measurements are done by a software called “ImageJ” and the procedure is explained below:

- Setting the scale of the image from pixels to micrometers by using scale bar in the original SEM image (Figure 11).

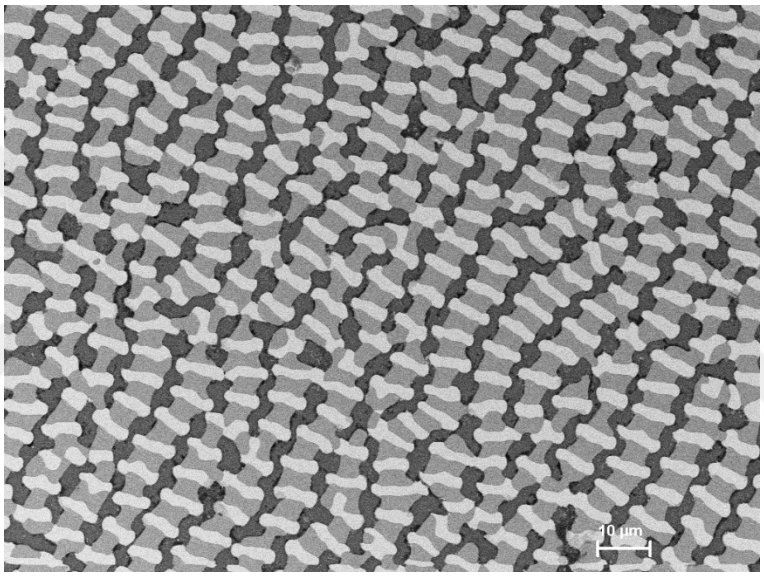

Figure 11. An example of SEM image from the cross-section of directionally solidified Al-Ag-Cu at V = 1.0 µm/s.

- Noise is despeckled to eliminate distinct small particles.
- Shadow and lines from SEM is filtered by applying “Extract background”, “Gaussian blur”.
- Brightness and contrast are adjusted. As a result image shown in Figure 12 is obtained.

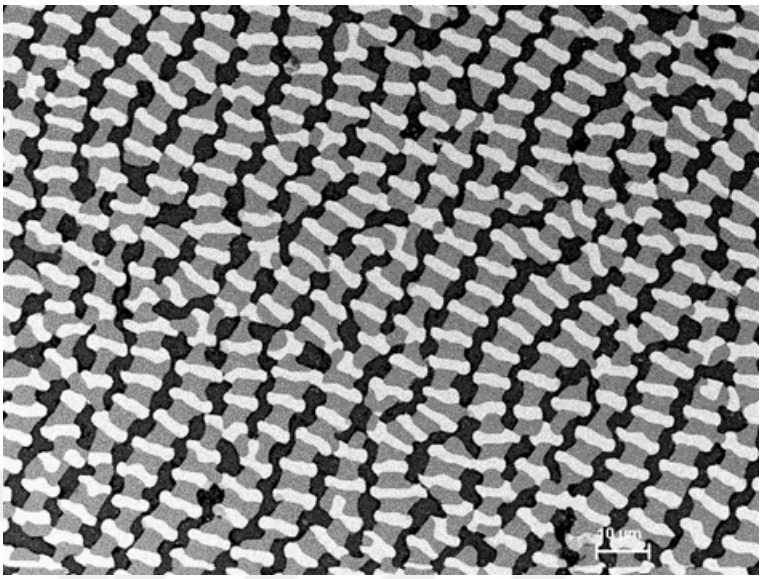

Figure 12. Image processed SEM image shown in Figure 11. (Improvements on image: Noise despeckle, brightness/contrast adjustment, and Gaussian blur).

- Binarizing the image by applying threshold and making interested particles (ex: Ag_2Al) white and rest is black as shown in Figure 13.
- The parameters are measured from each particle of the black & white image and the average values as well as the standard deviations are obtained.

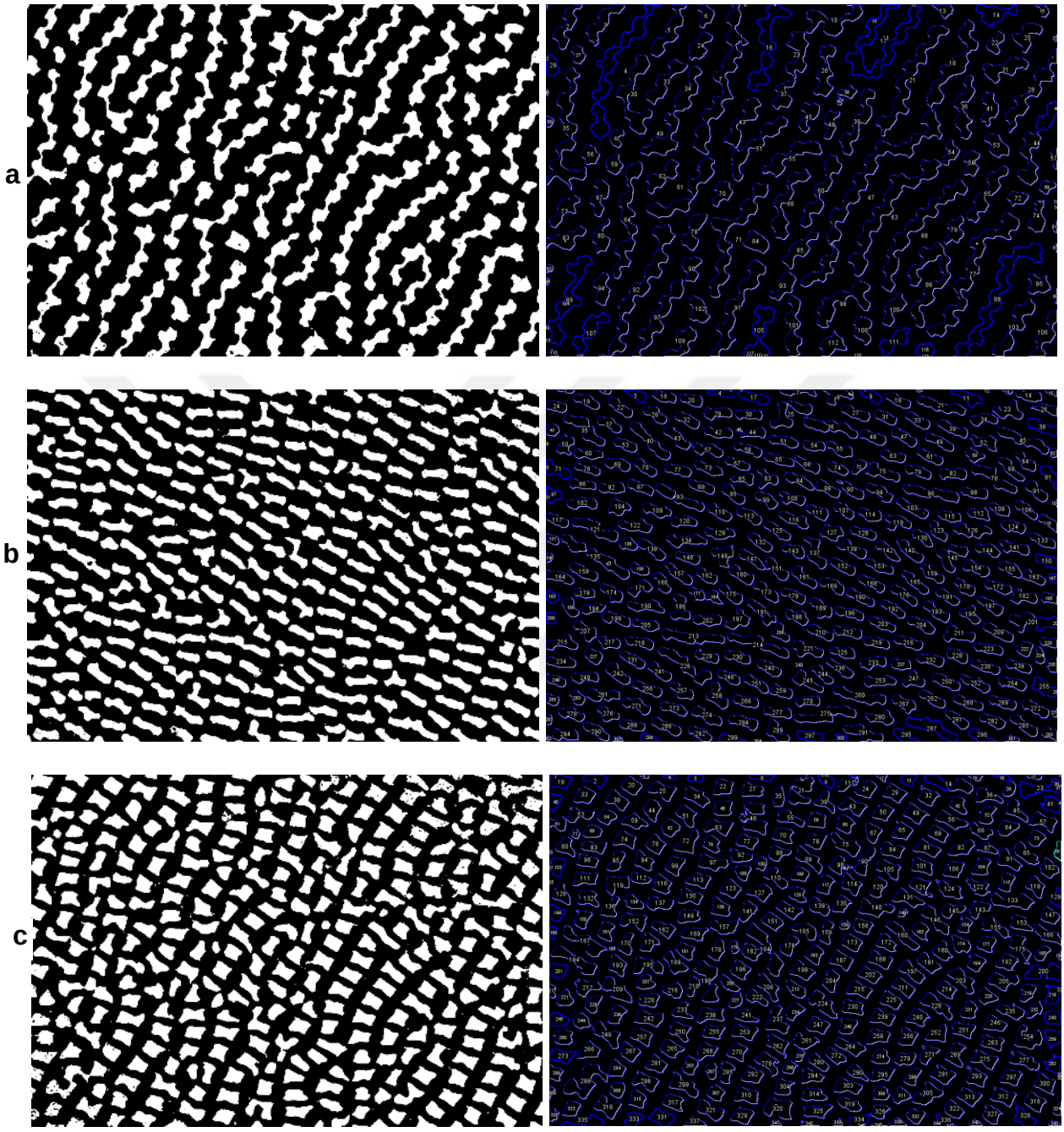

Figure 13. Binarized images and particles measured from the image shown in Figure 11 (a) (Al) particles converted to white and the outline of (Al) particles are shown, (b) Ag_2Al particles converted to white and outline of Ag_2Al particles are shown, (c) Al_2Cu particles converted to white and outline of Al_2Cu particles are shown.

While phase fraction is defined as the total area of one phase divided by total area of the image, the average particle area is measured by taking the average of each particle's area. Moreover, a method is developed to measure the eutectic spacing in this very complex microstructures. In this method, Feret Technique is used to calculate eutectic spacing and its details are explained in the following section.

2.6. Particle Based Measurement Technique Feret

According to Jackson-Hunt theory, the scale of the microstructure depends on the solidification velocity. This can be clearly observed from the SEM images taken from samples grown at different velocities but for the mathematical comparison, eutectic spacing must be measured. Therefore, Feret technique is implemented for the first time in the literature to measure eutectic spacing by using particles' widths and lengths.

Minimum Feret is the smallest distance between two parallel planes that squeeze the particle. Similarly, maximum Feret is the longest distance between two parallel planes that squeeze the particle as schematically shown in Figure 14a. Both maximum and minimum Feret values of each phase are plotted in a histogram graph and the average value is calculated by fitting the data in a Gaussian distribution and measuring the value at the peak frequency (Figure 14b). Therefore, two results (length and width) from three phases are obtained.

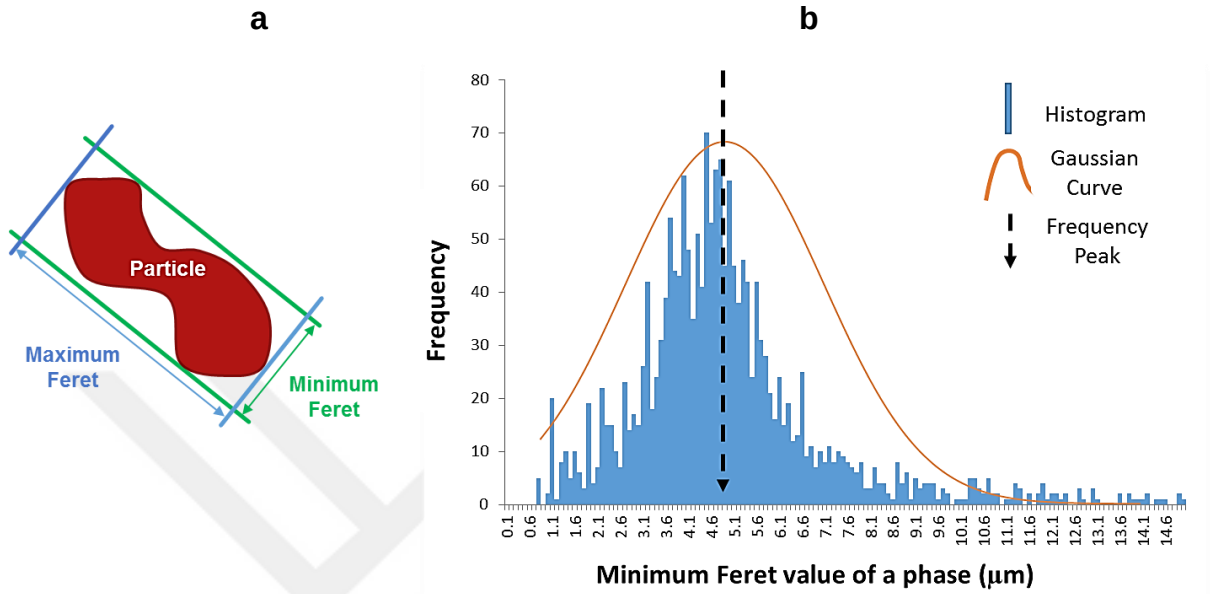

Figure 14. (a) Definition of minimum and maximum Feret, (b) An example of a histogram graph where the data belongs to particles from a phase, orange curve is the Gaussian fit the data and dashed line points out the average value.

Using these minimum and maximum Feret values, two eutectic spacing values namely, λ_1 and λ_2 (Equation 5, 6, 7) are defined to characterize the scale of this complex microstructure.

$$\lambda_1^{\alpha} = \alpha_{\text{max. Feret}} + \gamma_{\text{min. Feret}} \quad (5)$$

$$\lambda_1^{\beta} = \beta_{\text{max. Feret}} + \gamma_{\text{min. Feret}} \quad (6)$$

$$\lambda_2 = \alpha_{\text{min. Feret}} + \beta_{\text{min. Feret}} \quad (7)$$

Ag has high solubility in (Al) phase at high temperatures so that during solidification, the amount of Ag inside (Al) matrix phase is high. But as the temperature decreases, the solubility of Ag in (Al) phase decreases substantially and Ag elements rejected by (Al) phase is diffused to Ag_2Al phase. As a result, Ag_2Al phase start to enlarge into (Al) matrix phase after solidification (Figure 15a). In order to measure the eutectic spacing of solidification microstructure, the width of

both Ag_2Al and Al_2Cu phases are measured for λ_1 and named as λ_1^{α} and λ_1^{β} as shown in Figure 15. As a result, there is only one λ_2 value which is the sum of widths of alternating Ag_2Al and Al_2Cu phases named as ladder structure and there are two λ_1 for the width of ladder structure and width of (Al) matrix phase (Figure 15c).

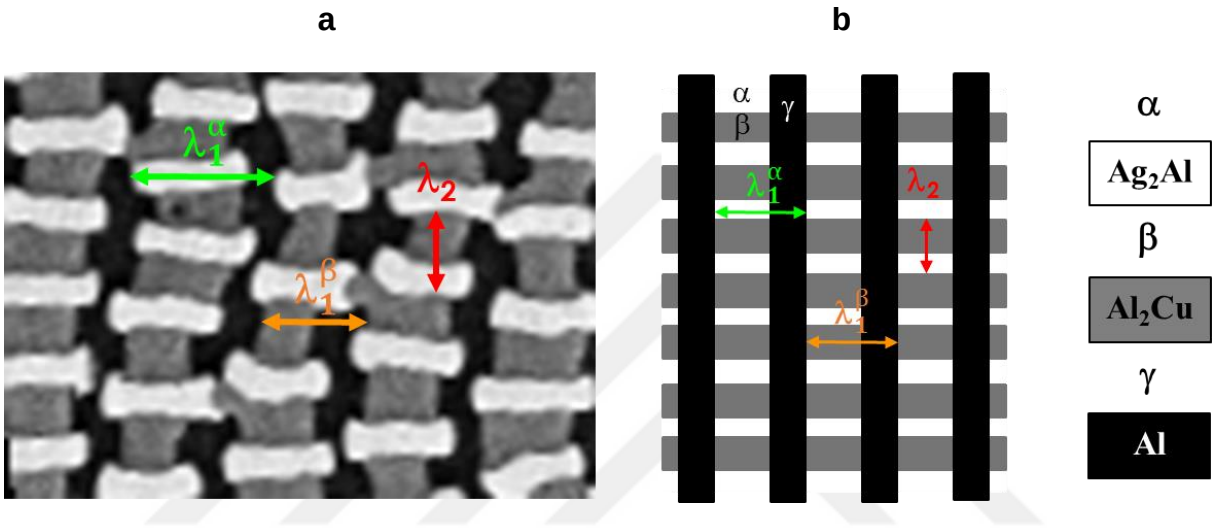

Figure 15. Definition of eutectic spacing, (a) An example SEM image from the cross-section of Al-Ag-Cu ternary eutectic alloy, (b) Normalized eutectic array.

3. RESULTS & DISCUSSION

Although there are many chain-like structure studies from Al-Ag-Cu eutectic system, different areas from one cross-section has been evaluated all the time instead of analyses of the whole cross-sectional area through the growth length. In this study, four main groups of microstructures were observed as a function of velocity and growth length which are summarized in the microstructure map shown in Figure 17. These microstructures are: chain-like structure, paw structure, faceted structure, and the microstructures obtained at the initial transient stage of solidification. Representative images of all these microstructures are shown in Figure 16.

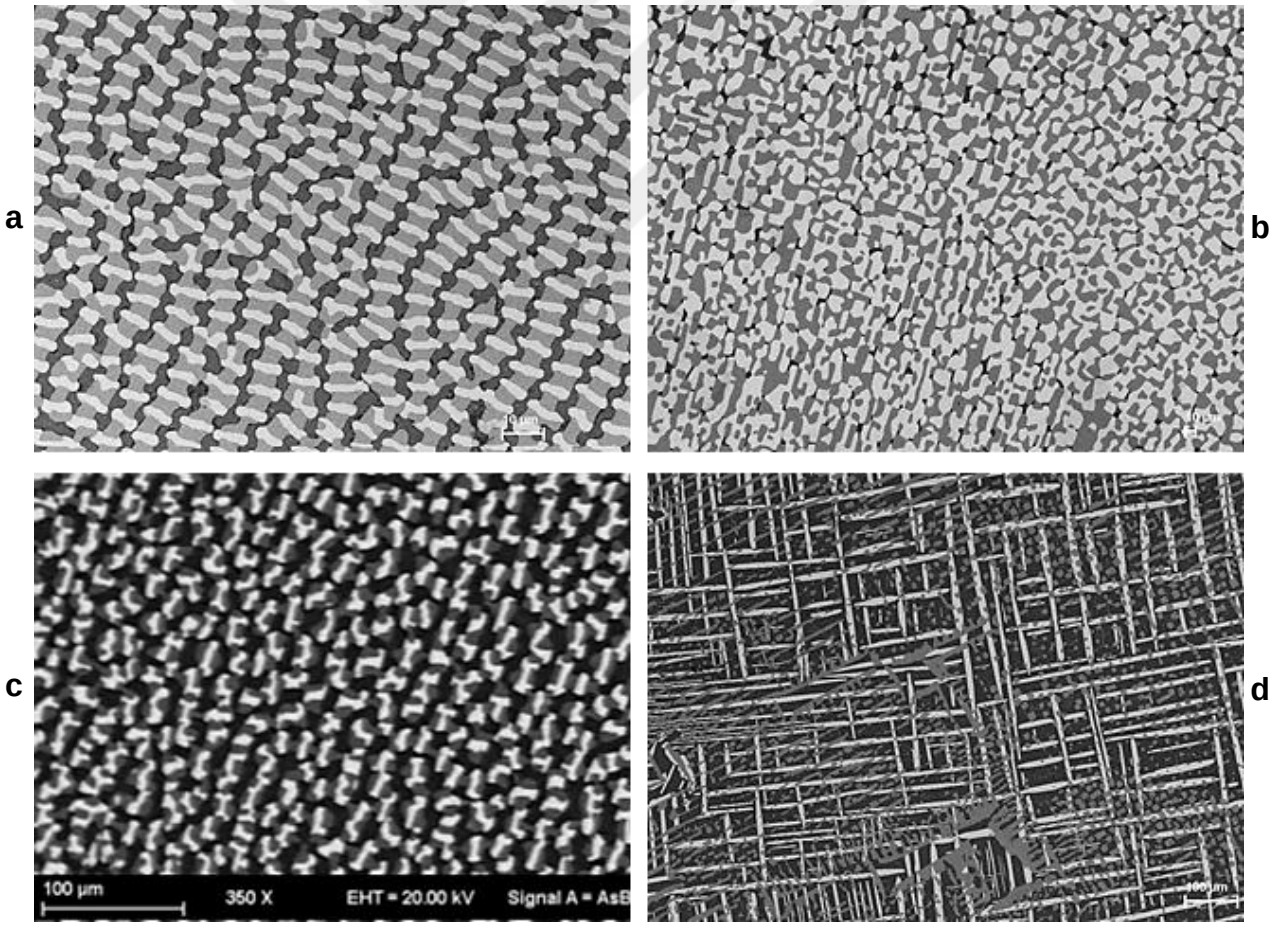

Figure 16. Cross-sectional SEM Images from four different microstructures (a) Chain-like structure, (b) Initial transient microstructure, (c) Paw structure, (d) Faceted structure.

Since eutectic solidification dynamics favor coupled growth, alternating arrangement of phases, which is chain-like structure for Al-Ag-Cu ternary system, has the biggest bubble area in velocity vs. growth length graph. Chain-like structure is observed at medium velocities and moderate growth lengths (Figure 16a). Distance to reach steady state is inversely proportional to solidification velocity so that at low velocities initial transient lasts longer. Therefore, initial transient microstructures are observed at low velocities like 0.1 μm/s and 1.0 μm/s and at low growth lengths (Figure 16b). Paw structure forms where Ag_2Al and Al_2Cu phases grow in rod-like shape instead of lamella between (Al) phases. Therefore smaller and circular intermetallic phases are obtained in a cross-sectional SEM image (Figure 16c). Faceted structure forms where the atoms attach to the solid by following specific plane orientations so that crystal grows in specific directions. In Al-Ag-Cu ternary system, it is observed that Ag_2Al and Al_2Cu phases grow with a specific shape and orientations (Figure 16d). Faceted structure and paw structure form as growth length increase. That is, faceted structure forms at Velocity (V) ≤ 0.5 μm/s and Growth Length (GL) ≥ 60 mm whereas paw structure is observed at V ≥ 1.5 μm/s and GL ≥ 60 mm. Since there is formation of paw and faceted structure along the growth, at some growth lengths they coexist with chain-like structure and these structures labeled with two letters in Figure 17. However, if one structure is observed, it is stated with single letter. There are also undetermined structures on the cross section of 5 mm diameter sample. However, the total are of the undetermined structure is less than 22% in case of initial transient and it is less than 7% for the rest of the structures. By using ImageJ, boundaries between the different structures are drawn and areas are measured. Then, in order to calculate the error, the ratio of the undetermined structure to whole cross-section is taken. For example, 95% of the cross-section is composed of faceted structure at V = 0.1 μm/s and growth length of 100 mm so that error is 5%.

Microstructures are characterized with a newly developed method, which involves Feret technique. By using this method, a new technique for measuring the eutectic spacing is suggested and the relationship between average eutectic spacing and directional solidification velocities as well as $\lambda^2 V$ values are measured. Similarly, particle areas and phase fractions are measured along the growth length.

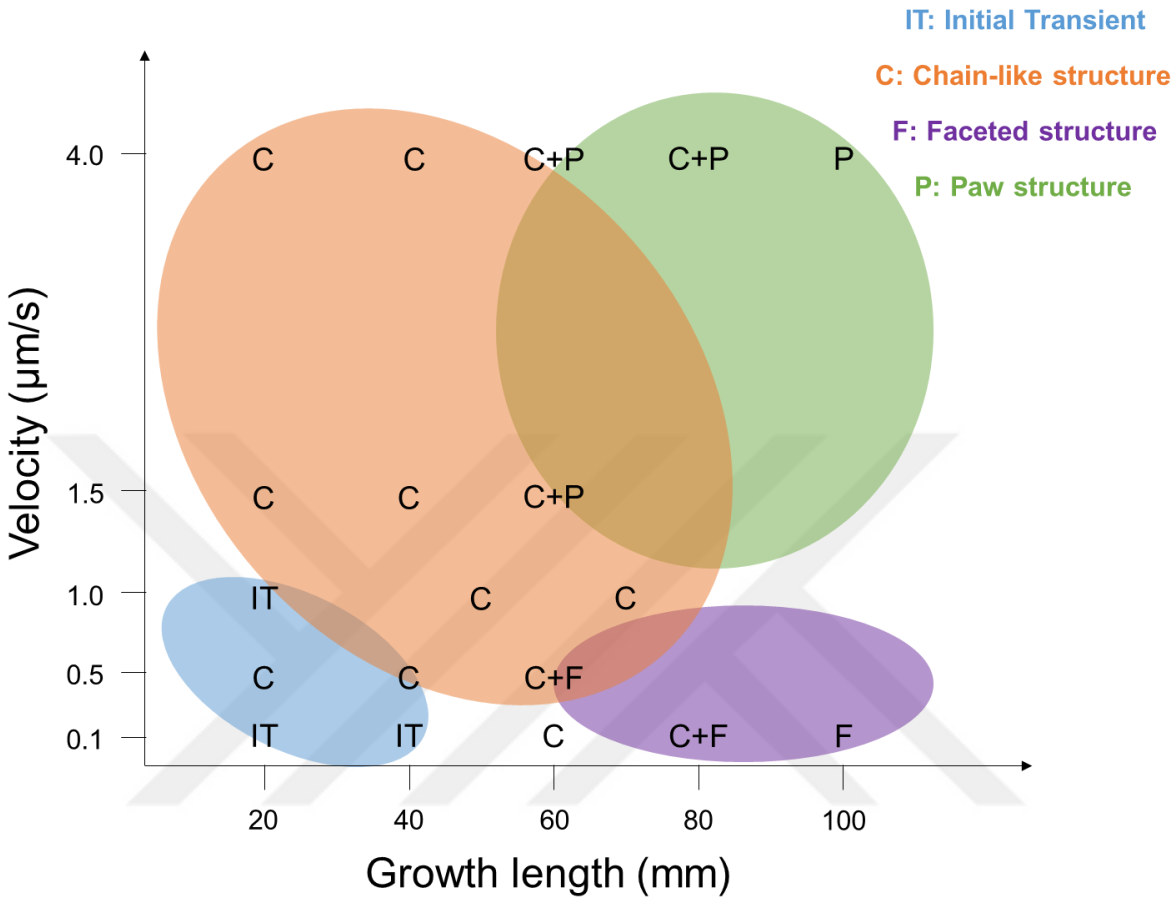

Figure 17. Directional solidification velocity vs. growth length graph. Colored bubbles represent different microstructures. Single letter shows one microstructure over the cross-section and double letter is for coexisting phases.

3.1. Microstructures of Directionally Solidified Al-Ag-Cu Eutectic System

In order to ensure that imposed temperature gradient is homogenous through the width of the sample, longitudinal analysis is essential to investigate the planarity of the S/L interface. In Figure 18, microstructure grown at V = 1.2 µm/s and quenched microstructure can be seen together. The interface between these two microstructures is planar although there is a slight curvature at the sides of the sample due to the surface tension between the walls and the alloy. Therefore, thermal gradient during directional solidification is sufficiently high to keep S/L interface planar by preventing formation of cell or dendrites. Cellular or dendritic microstructures can form when impurity atom rejection is not fast enough with a planar interface because planar interface

has a smaller S/L surface area compared to S/L areas of cellular or dendritic microstructures. By using elements with 99.999% purity level as well as high thermal gradient values at melting point provides planar S/L interface.

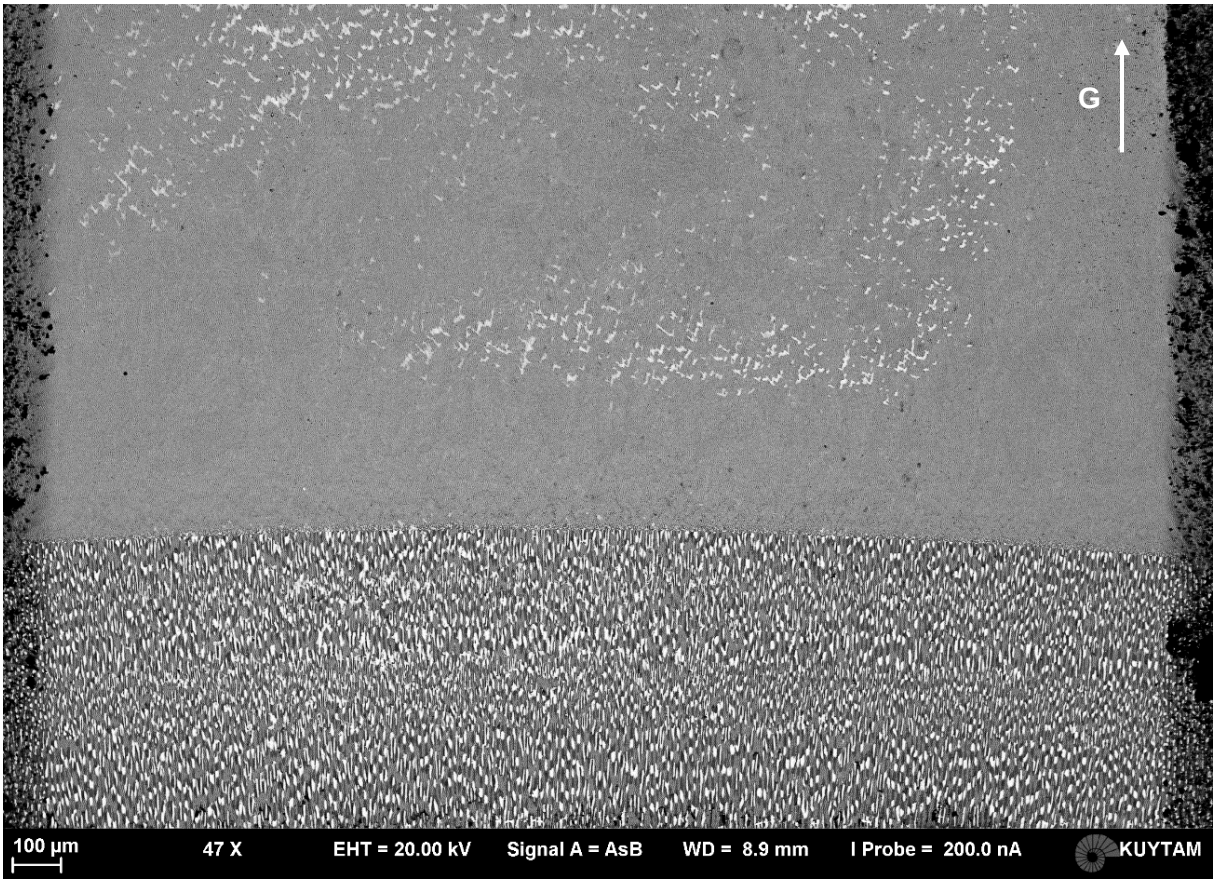

Figure 18. Longitudinal SEM image of directionally solidified (V = 1.2 µm/s) sample with 5 mm in diameter. Thermal gradient direction is shown by the white arrow.

After determination of the S/L interface position, sample is cut from 1 mm below the interface so that longitudinal and cross-sectional microstructure can be seen at the same time. Image shown in Figure 19 is important because solidification can be observed from both longitudinal and cross-sectional views and it provides a 3D perspective of a thick sample. Some changes are observed at the longitudinal view and the final microstructure is obtained at the cross-

sectional view. Black areas are Al_2Cu, gray areas are (Al) matrix and white areas are Ag_2Al phase whose details were explained in section 3.1.1.

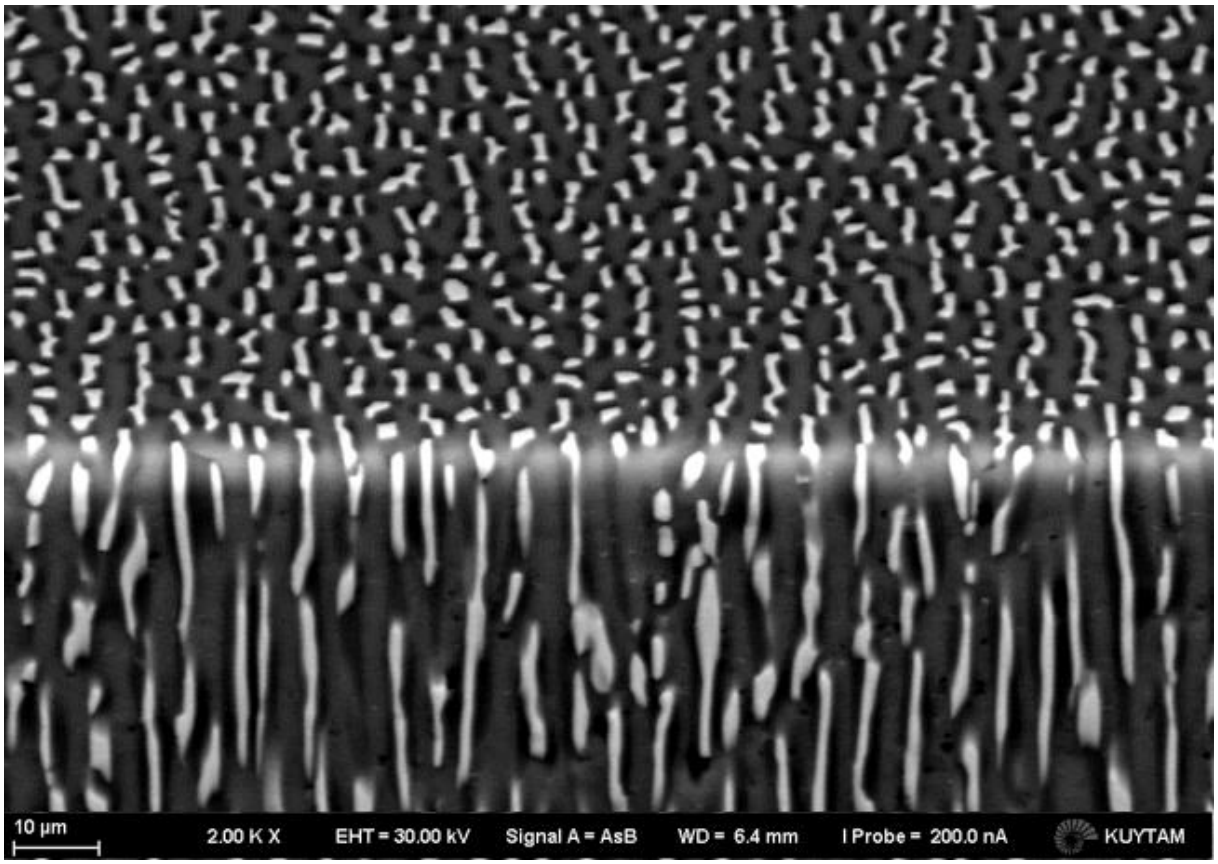

Figure 19. Longitudinal and cross-sectional views of the directionally solidified Al-Ag-Cu eutectic alloy (V = 4.0 µm/s). Image is taken 1 mm below the S/L interface and the sample diameter is 5 mm. Black area: Al_2Cu, gray area: (Al) matrix and white area: Ag_2Al.

The matrix phase is Al whereas Ag_2Al and Al_2Cu phases are rods with rectangular cross-sections. Longitudinal images present complex microstructural features since sample has a large diameter, which causes flexibility of motion in every direction. That's why, longitudinal investigation is difficult for the thick samples so that cross-sectional analysis are preferential for microstructural characterization. In the following sections, directionally solidified sample images from different diameter and velocities are presented.

3.1.1. Chain-like Structure

The eutectic microstructure obtained in Al-Ag-Cu ternary system is generally chain-like structure. Alternating Ag_2Al (white) and Al_2Cu (gray) phases form the ladder structure, whereas (Al) matrix phases are parallel to this structure.

In directional solidification experiments, different grains can have different array and even different microstructures. In Figure 20, cross-section image of directionally solidified (V = 1.5 μm/s) sample at growth length of 40 mm is seen. The grain boundary is marked by all dashed red curve as claret red and the array direction is represented by yellow dashed arrows. Although, there are some faults such as ring-like structure, Y junction, and dead end, the array is regular in a very large area within a grain. Ring-like structure is observed where the two-phase lamellae of the intermetallic phases are arranged to a circle in 2D or a tube and a spiral in 3D. Y junction faults form when two different particles of the neighboring two-phase lamellae are broadened and touch each other. Dead end is observed when the alteration of Ag_2Al and Al_2Cu along the ladder structure finishes by (Al) matrix phase [28].

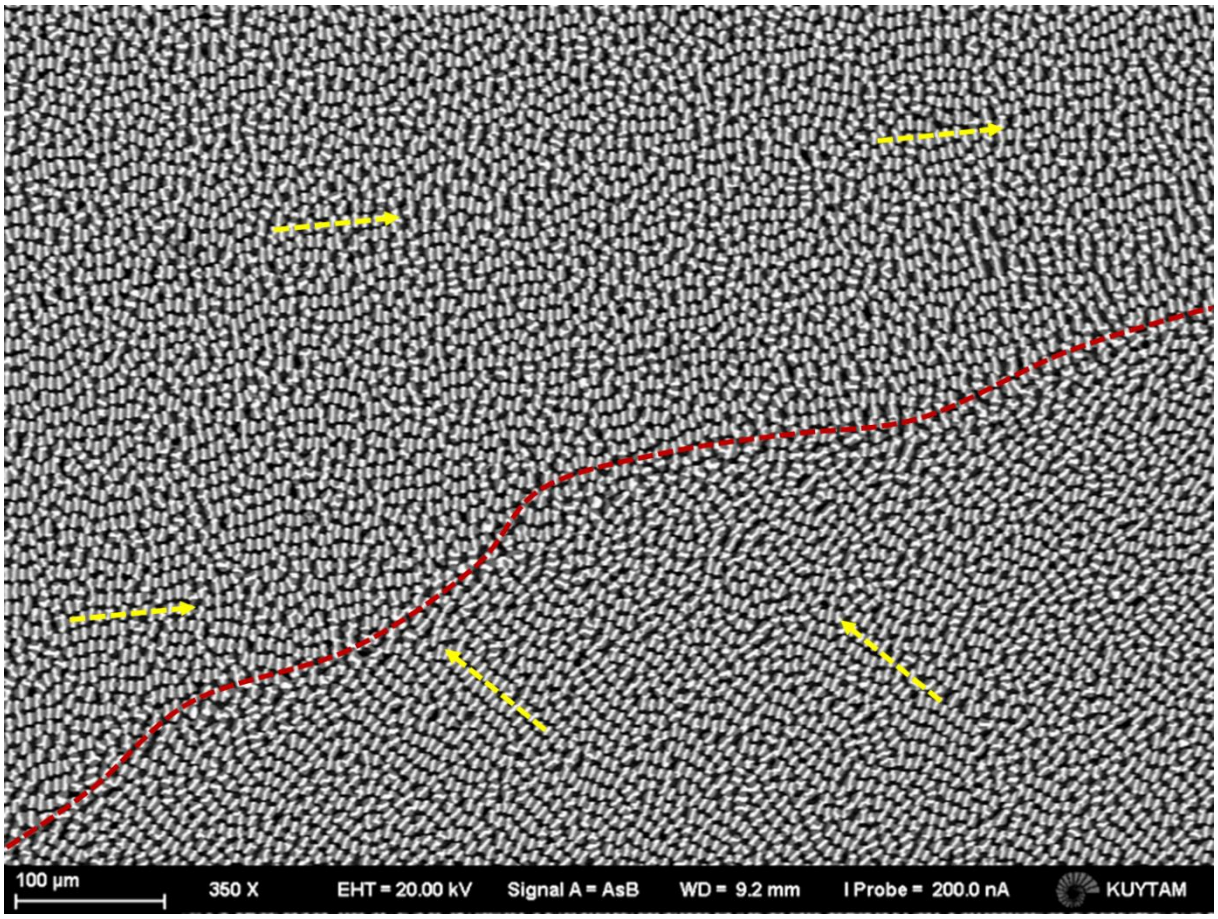

Figure 20. SEM image of directionally solidified (V = 1.5 µm/s) sample. Growth length is 40 mm and the diameter of the sample is 5 mm. Dashed red line shows the grain boundary and array directions in the grains are represented by yellow dashed lines.

Another example of chain-like structure with a higher magnification is presented in Figure 21. The microstructure is very regular and the direction of the phases are similar because the image is taken from one single grain.

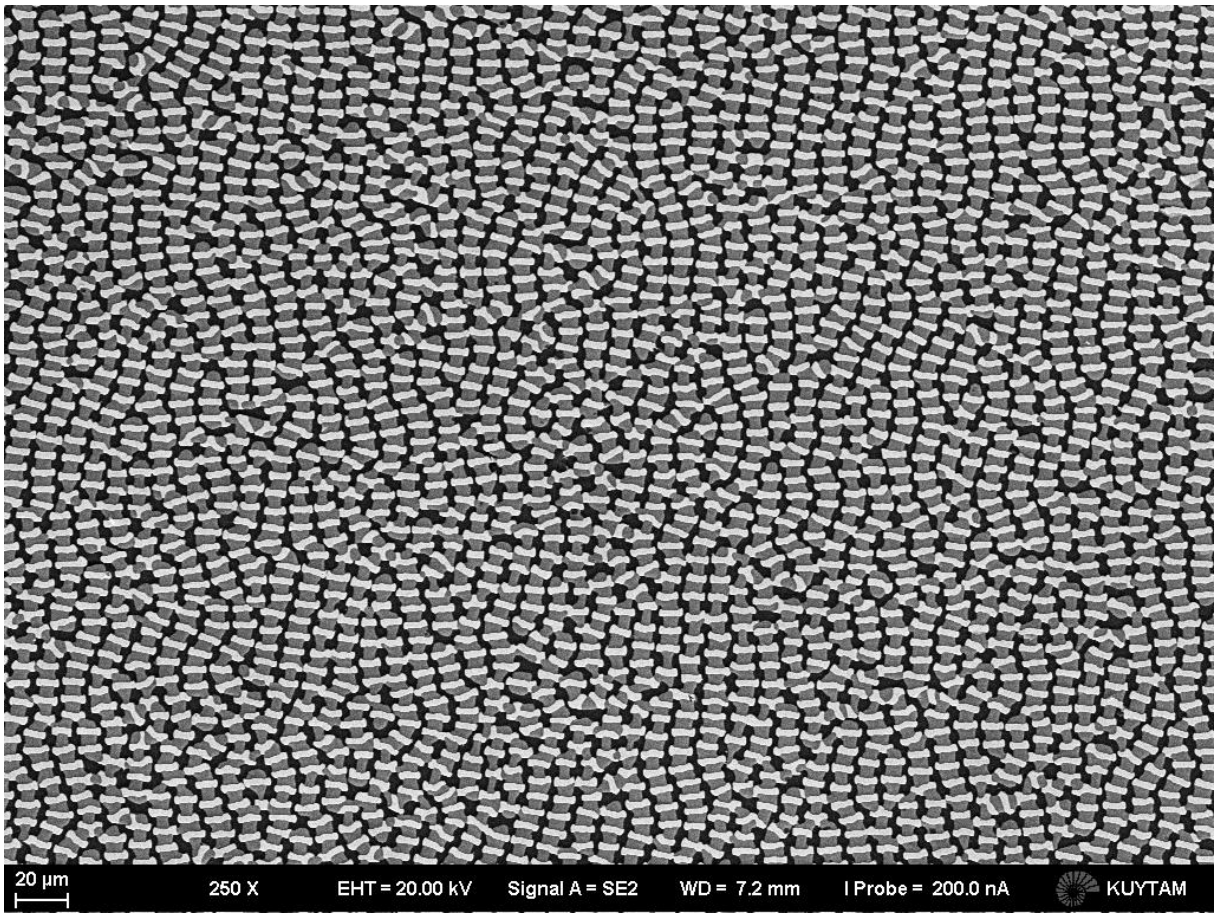

Figure 21. Chain-like structure observed at 17 mm growth length. Black area is Al phase, gray area is Al_2Cu, and white area is Ag_2Al. Directionally solidified Al-Ag-Cu sample with 5 mm in diameter (V = 1.2 µm/s).

Velocity dependence of the microstructure is demonstrated in chain-like structures. For instance, in Figure 22, four images from microstructures formed at V = 1.0 µm/s, 1.2 µm/s, 1.5 µm/s, and 4.0 µm/s at the same magnification (250x) show that finer microstructure is obtained as velocity increases.

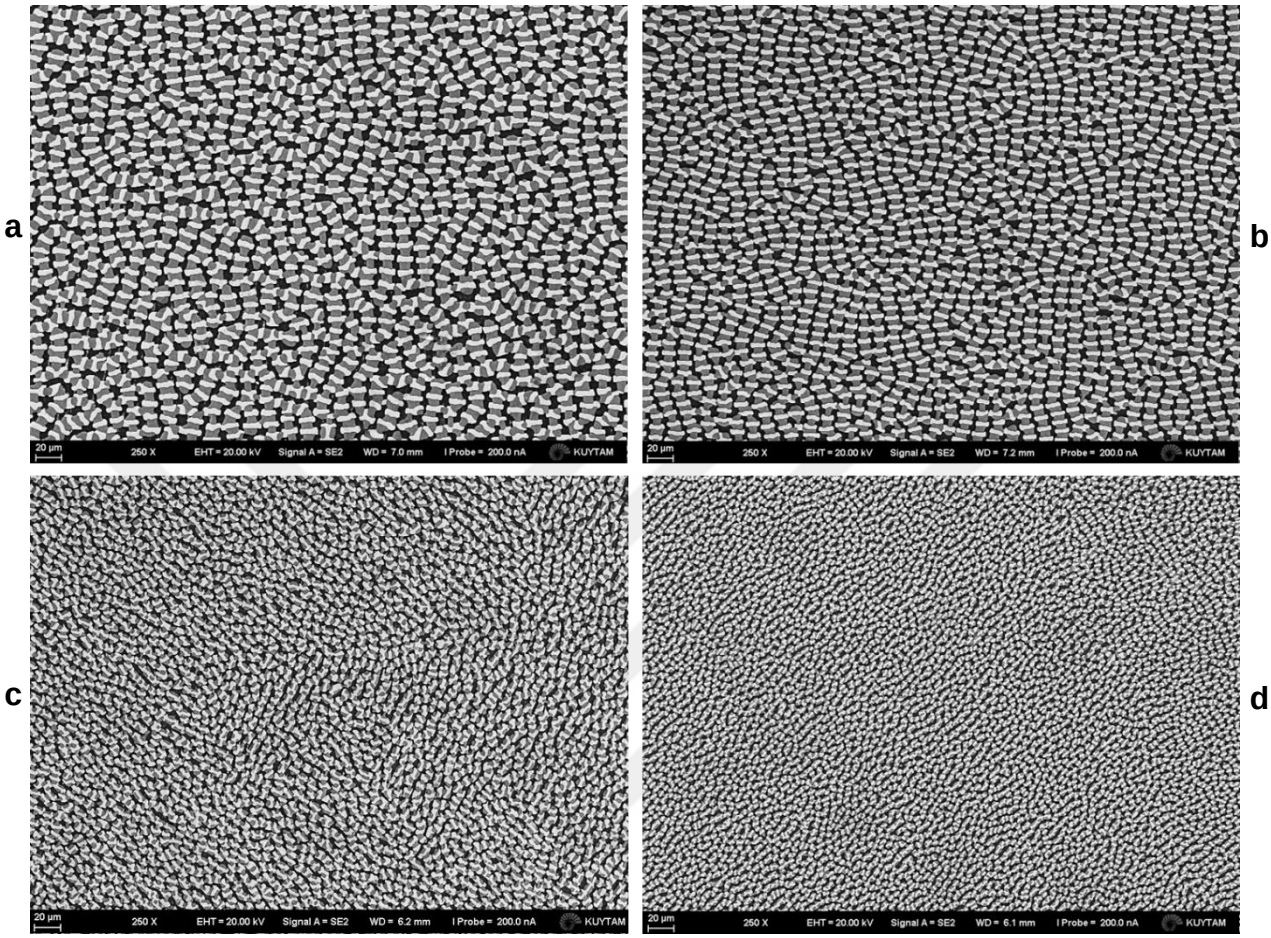

Figure 22. SEM images of directionally solidified samples with (a) 1.0 µm/s, (b) 1.2 µm/s, (c) 1.5 µm/s, (d) 4.0 µm/s at 250x magnification. All sample diameters are 5 mm.

These microstructures are characterized by using the new method, which includes Feret technique to calculate eutectic spacing. Additionally, as phase fraction and particle area analysis are done. In Table 2, eutectic spacing values, phase fractions, and area analysis corresponding to the SEM images shown in Figure 22 are presented. There is a certain decrease in eutectic spacing and average particle size, while phase fractions are very close to each other. That is, phase distribution is constant and number of particles increases at high velocity experiments in order to lower the eutectic spacing values such that they will stay within the limits of stability (Figure 23).

Table 2. Velocity and eutectic spacing, phase fraction and average particle area values measured from chain-like structures.

V (μm/s)	λ_1^{α} (μm)	λ_1^{β} (μm)	λ_2 (μm)	Phase Fraction (%)			Average Phase Area (μm²)		
				(Al)	Al_2Cu	Ag_2Al	(Al)	Al_2Cu	Ag_2Al
1.00	18.06	14.01	8.77	26.24	36.50	37.26	59.30	19.68	33.51
1.20	15.78	12.38	7.38	26.09	37.20	36.71	38.71	16.73	26.05
1.50	12.55	9.82	6.92	30.96	35.52	33.52	25.44	10.58	17.34
4.00	7.58	5.14	4.29	24.22	36.93	38.85	5.42	3.66	7.51

Graphs are drawn by values in the table for both eutectic spacing and area analysis at changing velocity.

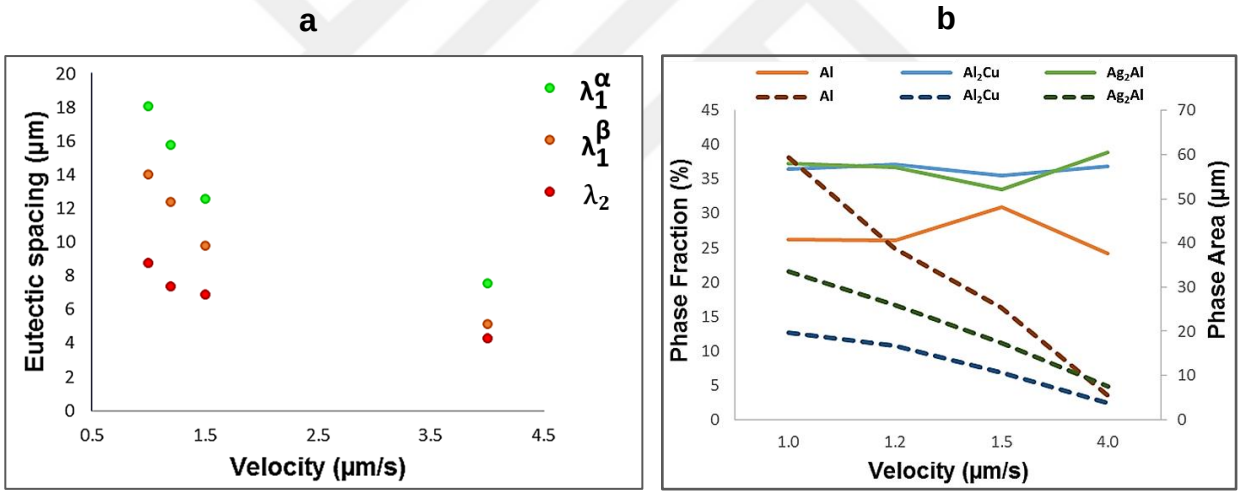

Figure 23. (a) Eutectic spacing vs. velocity graph, (b) phase fraction (solid lines) and phase area (dashed lines) vs. velocity graph. Data is taken from Table 2.

3.1.2. Paw Structure

At relatively high velocities, the length of (Al) matrix phase increase and the arrangement of Ag_2Al and Al_2Cu changes with increase in growth length. This change is the transformation from chain-like structure to paw structure. In Figure 24, directional solidification at 4.0 μm/s velocity is investigated from different growth lengths. Completely chain-like structure at growth length of 40 mm, transforms partially to paw structure at 60 and 80 mm growth length. At 100 mm growth, however, it is completely paw structure.

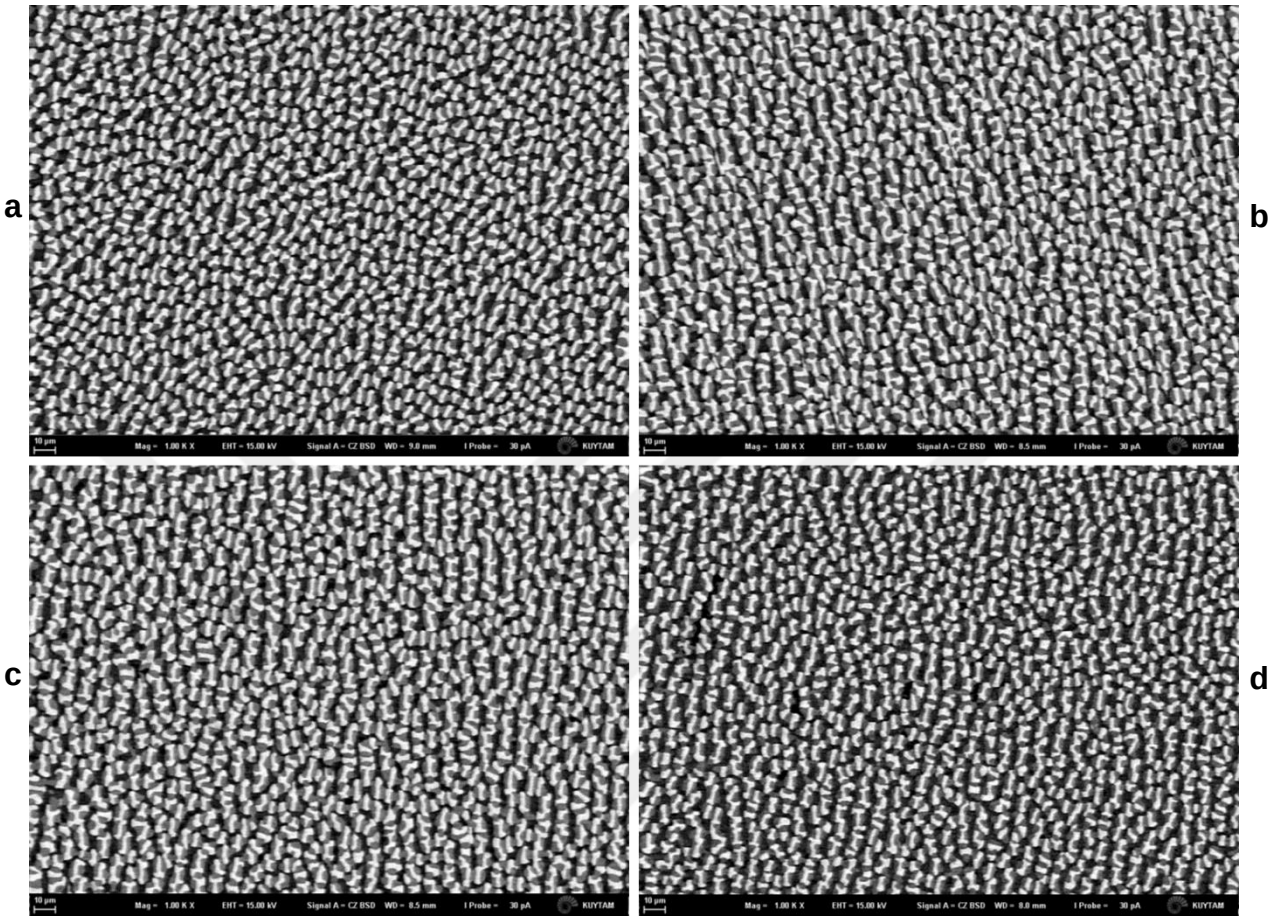

Figure 24. The transformation of directionally solidified (V = 4.0 μm/s) sample along growth length. Sample diameter is 5 mm. (a) Completely chain-like structure at 40 mm growth length (b) mostly chain-like structure at 60 mm growth length (c) mostly chain-like structure at 80 mm growth length (d) completely paw structure at 100 mm growth length. Images are at the same magnification (1000x).

Similarly, as it is presented in Figure 25, the same transformation is observed for directionally solidified (V = 1.5 μm/s) sample.

a 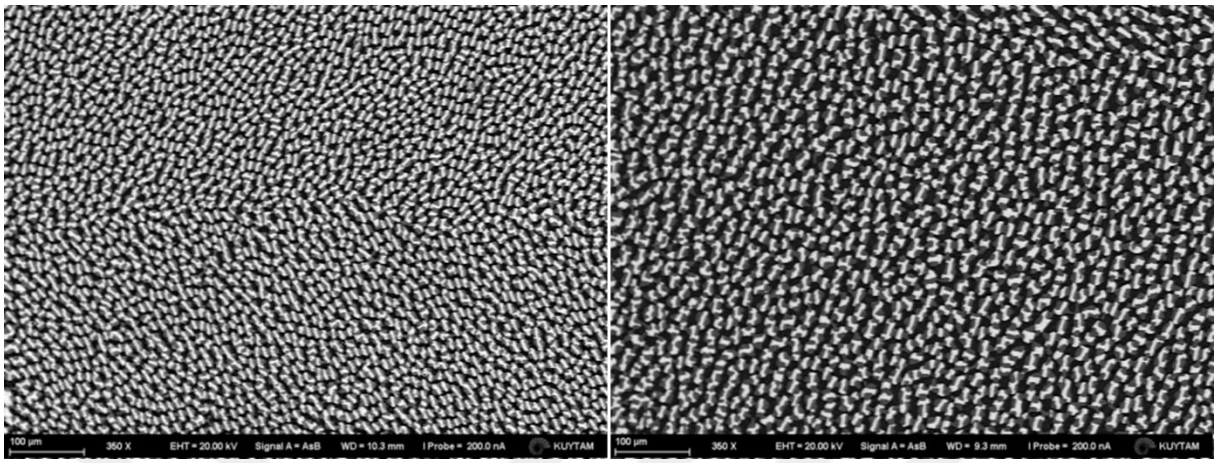 b

Figure 25. The transformation of directionally solidified (V = 1.5 μm/s) sample along growth length. Sample diameter is 5 mm. (a) Completely chain-like structure at 20 mm growth length (b) Completely paw structure at 60 mm growth length. Images are at the same magnification (350x).

Whole cross-section of directionally solidified (V = 1.0 μm/s) sample at 50 and 70 mm growth lengths are examined and having more than 93% chain-like structure on the cross-section proves that paw structure formation occurs V ≥ 1.5 μm/s.

Newly-developed eutectic spacing measurement method which involves Feret technique is implemented for the microstructures grown with V = 1.5 μm/s and V = 4.0 μm/s. Through the transformation from chain-like structure to paw structure, eutectic spacing values increase as shown in Table 3. This is due to the formation of more circular Ag_2Al and Al_2Cu phases as well as longer and wider (Al) matrix phase.

Table 3. Comparison of eutectic spacing values between chain-like and paw structures at the same growth velocity and different growth lengths.

Velocity (μm/s)	Growth Length (mm)	Microstructure	λ_1^{α} (μm)	λ_1^{β} (μm)	λ_2 (μm)
1,5	20	Chain-like Structure	12.10	10.16	6.37
	60	Paw Structure	18.17	16.87	9.44
4,0	80	Mostly Chain-like Structure	8.20	6.53	4.73
	100	Paw Structure	10.94	8.51	5.01

3.1.3. Initial Transient Microstructure

Solute concentration in the liquid is piled up at the S/L interface due to the rejection of solute atoms. Until the steady state, initial transient continue. The growth distance to reach the steady state (z) depends on, diffusion coefficient, D, solidification velocity, V, and partition coefficient, k (Equation 9) [37].

$$Z = \frac{4D}{Vk} \qquad (9)$$

For instance, according to the calculations by using equation 9, 105.98 mm is needed to be grown to pass initial transient at 0.5 μm/s. However, steady state microstructure is observed at lower growth lengths. Although, this can be due to miscalculations in diffusion or partition coefficients, or kinetics in different solidification conditions, inversely proportional relationship is still valid. Therefore, at low velocity experiments, it is expected to have initial transient microstructure for longer growth lengths.

In Figure 26, the microstructure is composed of mostly Ag_2Al and Al_2Cu phases. The third phase which is (Al) is very rarely seen because the solute pile up is insufficient to form the three phase eutectic microstructure.

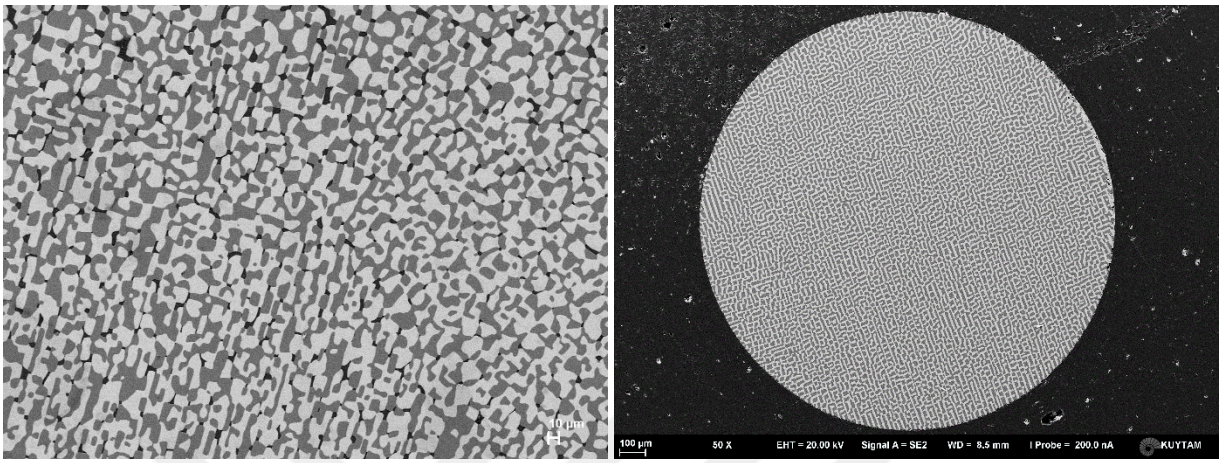

Figure 26. Initial transient microstructures of directionally solidified (V = 0.1 µm/s) sample (a) at 20 mm growth length, D = 5 mm (b) 40 mm growth length D = 1.5 mm. Black area is (Al) matrix, gray area is Al_2Cu and white area is Ag_2Al phase.

3.1.4. Faceted Structure

The microstructures of 60, 80 and 100 mm growth length after directionally solidified sample at V = 0.1 µm/s are presented in Figure 27, Figure 28 and Figure 29. These images are clearly showing the competition among the grains. At 60 mm growth length, at some regions chain-like structure is observed whereas the structure is irregular at the center.

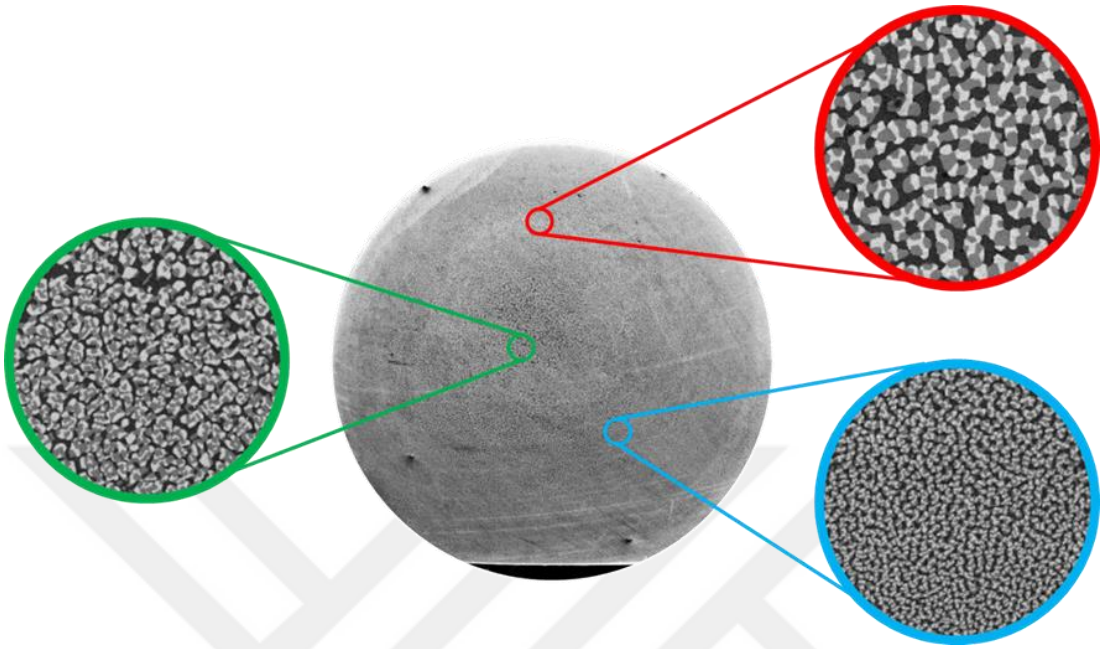

Figure 27. SEM image of directionally solidified sample (V = 0.1 μm/s). Cross-section is at 60 mm growth length and sample diameter is 5 mm. Whole sample image at the center is taken with 50x magnification, bottom right and left images are taken with 500x magnification and top right image is taken with 1000x magnification.

Unlike 60 mm growth length, chain-like structure is observed almost nowhere in the microstructure at 80 mm growth length (Figure 28). However, there exist different microstructures with sharp edges. The structure at the center of the sample has not been reported before. Therefore, it is named as faceted structure due to its sharp edges locked to some specific directions. There are long Ag_2Al needles in (Al) matrix whereas Al_2Cu phase is evenly distributed over the microstructure.

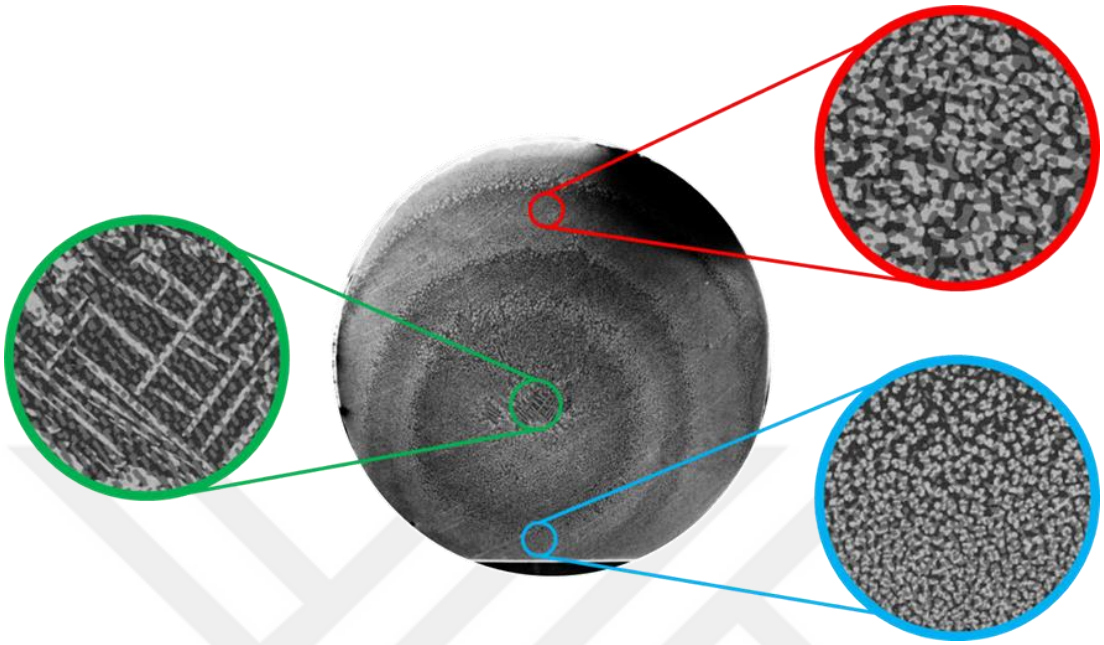

Figure 28. SEM image of directionally solidified sample (V = 0.1 μm/s). Cross-section is at 80 mm growth length and sample diameter is 5 mm. Whole sample image at the center is taken with 50x magnification, bottom right and left images are taken with 500x magnification and top right image is taken with 1000x magnification.

At 100 mm growth length, it is observed that the faceted grain wins the grain competition and spreads all over the sample except a very small area of 1.51 mm^2 (Figure 29).

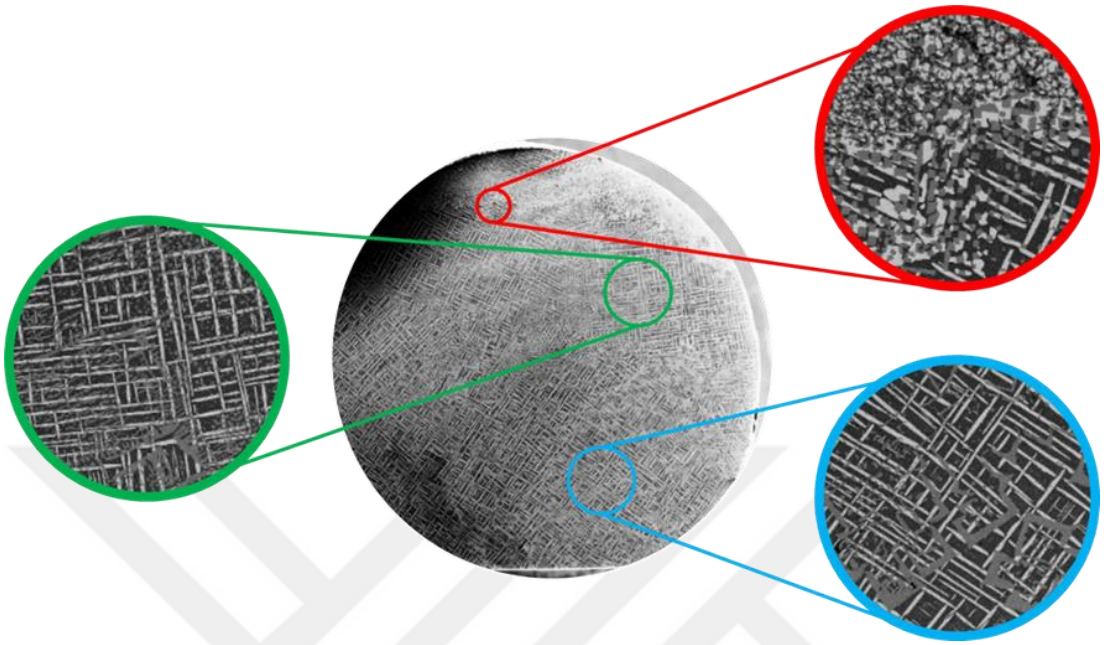

Figure 29. SEM image of directionally solidified sample (V = 0.1 μm/s). Cross-section is at 100 mm growth length and sample diameter is 5 mm. Whole sample image at the center is taken with 50x magnification, bottom right and left images are taken with 250x magnification and top right image is taken with 500x magnification.

3.1.4.1. EBSD Analysis

In order to understand the origin of this faceted structure, EBSD analysis are performed. SEM image of a faceted structure is presented in Figure 30a. Ag_2Al particles within (Al) matrix phase grow locked to the some specific directions, which is due to interphase anisotropy between (Al) and Ag_2Al phases. The EBDS analysis shown in Figure 30b shows that here are four orientations of Ag_2Al crystals and these Ag_2Al particles with different orientations are crossing each other. Since within a grain, all the crystals belonging to the same phase has to have the same crystal orientation, observation of different crystals crossing each other suggests that this microstructure is not obtained upon solidification. This formation is possible by post-solidification reaction like precipitation where Ag_2Al phase nucleates over (Al) phases.

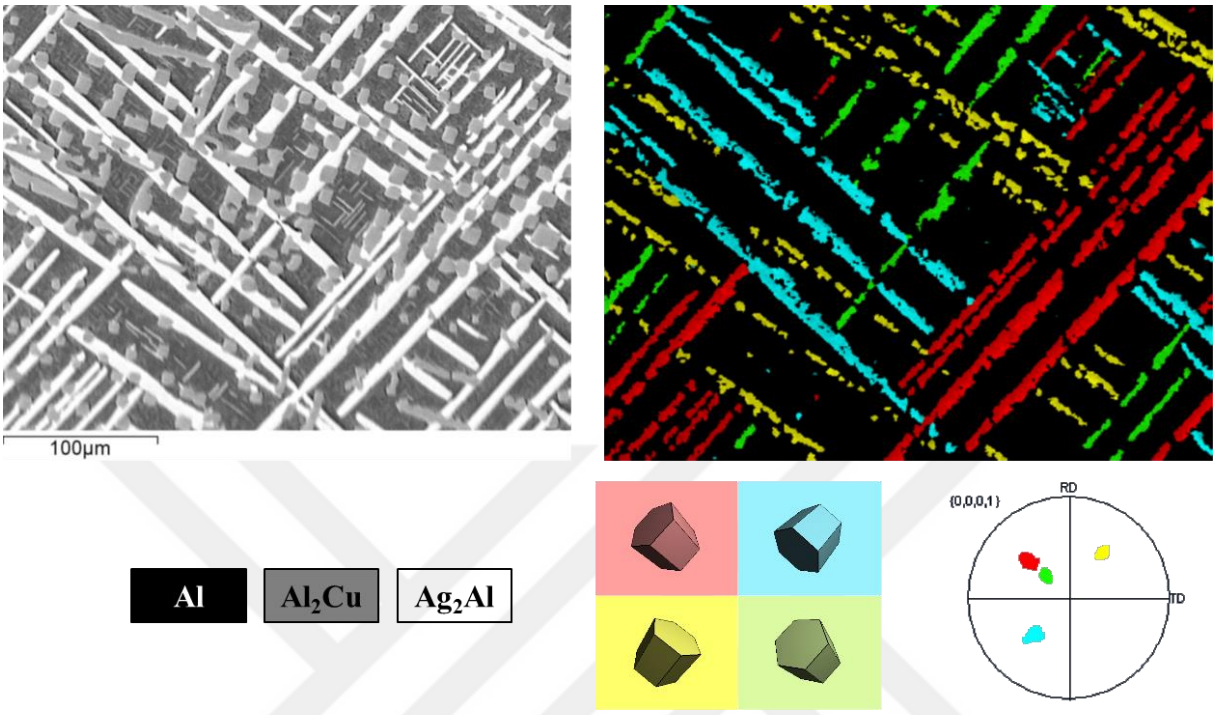

Figure 30. EBSD analysis of the faceted structure (a) Faceted structure grown at V = 0.1 µm/s (b) EBSD results of faceted structure with Ag_2Al crystal orientations.

3.1.4.2. ICP-MS Test

In order to understand why precipitation occurred in this low velocity, high growth length regime, chemical characterization of the sample is made. Directional solidification at V = 0.1 µm/s takes 330 hours for 120 mm growth length. That is, the sample stay in molten state for sufficiently long time as a result of which segregation occurs due to gravity. The density of Ag higher than Al; and that's why the main segregating element is expected to be Ag. To verify this and to determine the elemental composition of directionally solidified (V = 0.1 µm/s) sample, inductively coupled plasma mass spectroscopy (ICP-MS) technique is employed. For the comparison, as cast sample and directionally solidified sample at 120 mm growth length are tested (Table 4). Comparison of eutectic composition and 120 mm growth length sample shows that the shift is 4.3 at. % and 3.0 at. % for Cu and Ag respectively whereas 7.3 at. % increase is observed for Al.

Table 4. Elemental compositions obtained from ICP-MS test in atomic and weight percentages. 0 represents as cast state and 120 is the sample taken from 120 mm growth length.

	Growth Length	Al (%wt)	Cu (%wt)	Ag (%wt)	Al (%at)	Cu (%at)	Ag (%at)
ICP Results	**0**	37.70	19.02	43.28	66.61	14.27	19.12
	120	48.70	12.76	38.55	76.38	8.50	15.12
Reference [38]	**$C_{Eutctic}$**	40.26	17.57	42.16	69.10	12.80	18.10
		Al	**Cu**	**Ag**			
Reference [39]	**Density (Room Temperature)**	2.7	8.9	10.5			

3.1.4.3. DSC Test

Differential scanning calorimetry (DSC) test is used for determination of transformation temperatures of the sample at 120 mm growth length. Even though eutectic temperature of Al-Ag-Cu ternary eutectic alloy is 501 ºC, onset temperature of the transformation upon cooling obtained from DSC test is 550 ºC as it is presented in Figure 31. Onset temperature is the start of releasing energy in the graph, which corresponds to the start of nucleation. In addition, the onset of the second heat flow peak is at 501 ºC which is the eutectic temperature. Therefore, the start of solidification being at 550 ºC instead of eutectic temperature proves that the alloy composition is not at eutectic point.

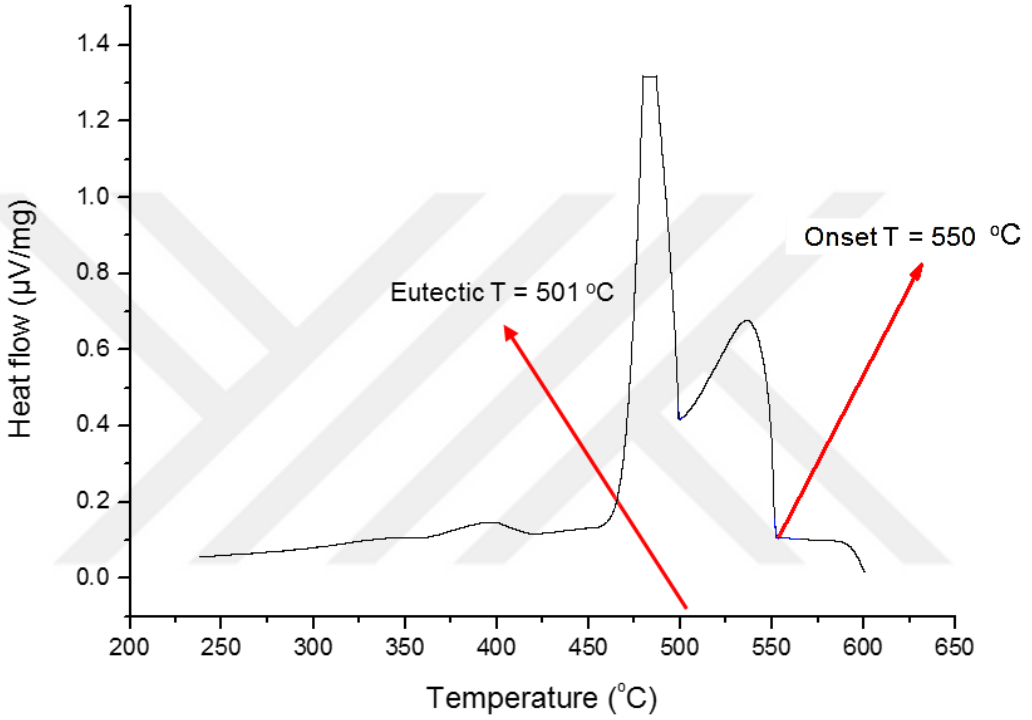

Figure 31. DSC thermograph of directionally solidified (V = 0.1 μm/s) sample at 120 mm growth length showing the start of solidification is at 550 ºC.

The results for 120 mm growth length sample obtained from ICP-MS (76.38 at. % Al, 8.50 at. % Cu, 15.12 at.% Ag) and DSC (823 K isotherm) test are matching at a specific point shown by black point on the Al-Ag-Cu ternary phase diagram (Figure 32). At this point, solidification starts with (Al) phase and three phase eutectic structure only forms when temperature reaches below 501 ºC. This shows that liquid is enriched in Al while Ag and Cu elements segregated at lower region of the sample.

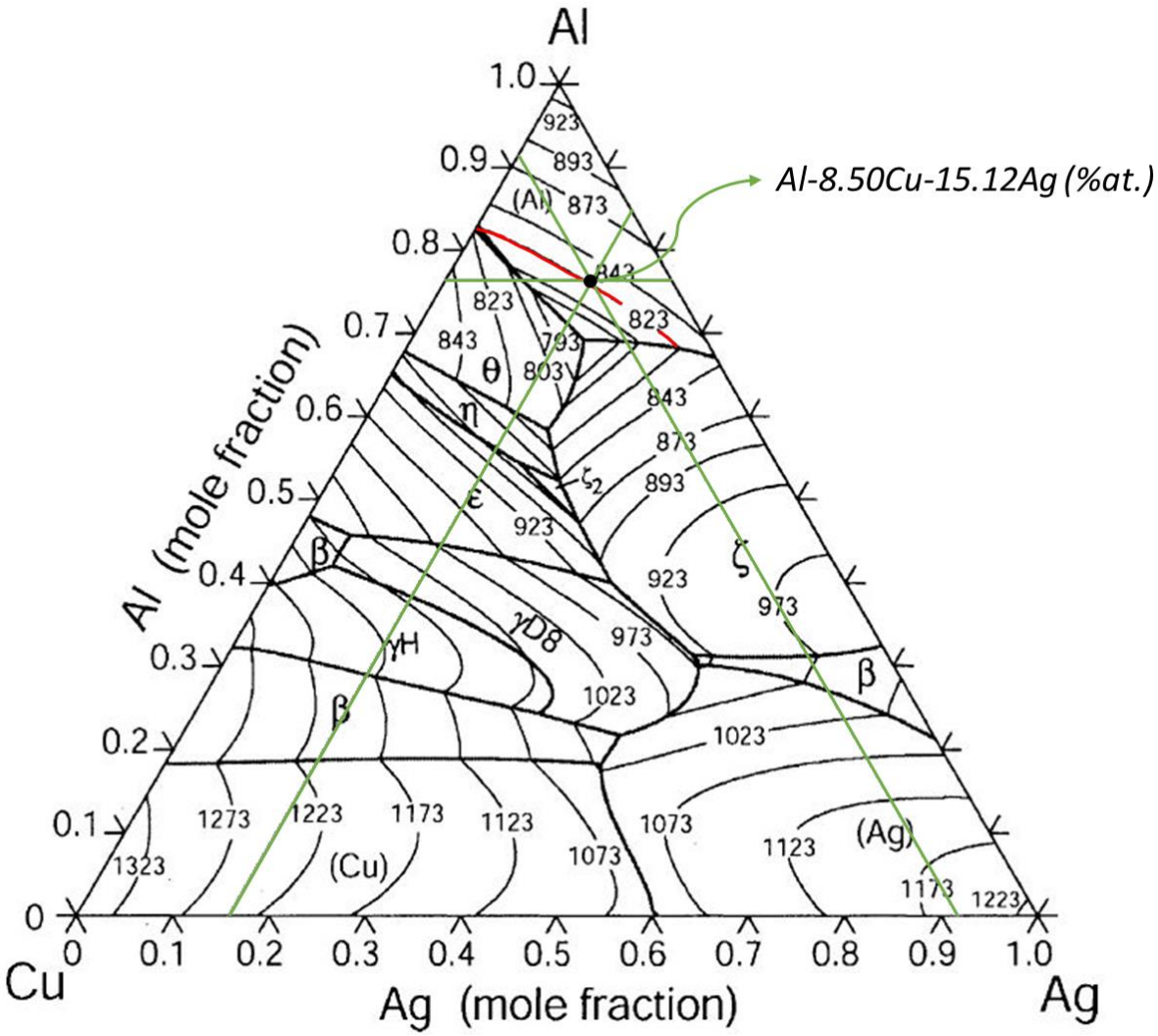

Figure 32. Al-Ag-Cu ternary phase diagram. Isotherm obtained from DSC test is represented by red line and elemental results obtained from ICP test are represented by green line [38].

As a result, segregation of Ag and Cu whose densities are much higher than Al takes place in the experiment which was run for 330 hours. Although, chain-like structure is obtained at low growth lengths, transformation to faceted structure is observed at GL ≥ 80 mm for the sample grown with V = 0.1 μm/s. Similarly, faceted structure is obtained in the sample grown with V = 0.5 μm/s after GL = 60 mm. Observation of faceted structure at higher growth lengths of lower velocity also shows that the main reason diffusion of the atoms with time due to gravity.

3.1.5. Sample Size Effect on Microstructure

Thermo-solutal convection in the liquid may also have an effect on the segregation. In order to understand this effect and to check if one can slow down the segregation, sample size is decreased to 3 and 1.5 mm diameters. This decrease will also result in decrease in the amount of liquid ahead of the S/L interface. Since casting of 1.5 mm diameter sample is difficult, alumina tube with inside diameter of 1.5 mm is placed into 5 mm rod cavity and molten alloy is poured into the mold. After casting, for the complete filling of the alumina tube with 1.5 mm diameter, mold is vertically placed into a furnace at 700 ºC. Afterwards, directional solidification is accomplished at V = 0.1 μm/s and common procedure for metallography is applied. SEM image obtained at 40 mm growth length shows that initial transient microstructure holds and white and gray phases formed both inside and outside of the alumina tube. (Figure 33). The regularity observed inside the alumina tube proves that there is a single grain at 40 mm growth length whereas a sample with 5 mm in diameter can have more than 5-6 grains.

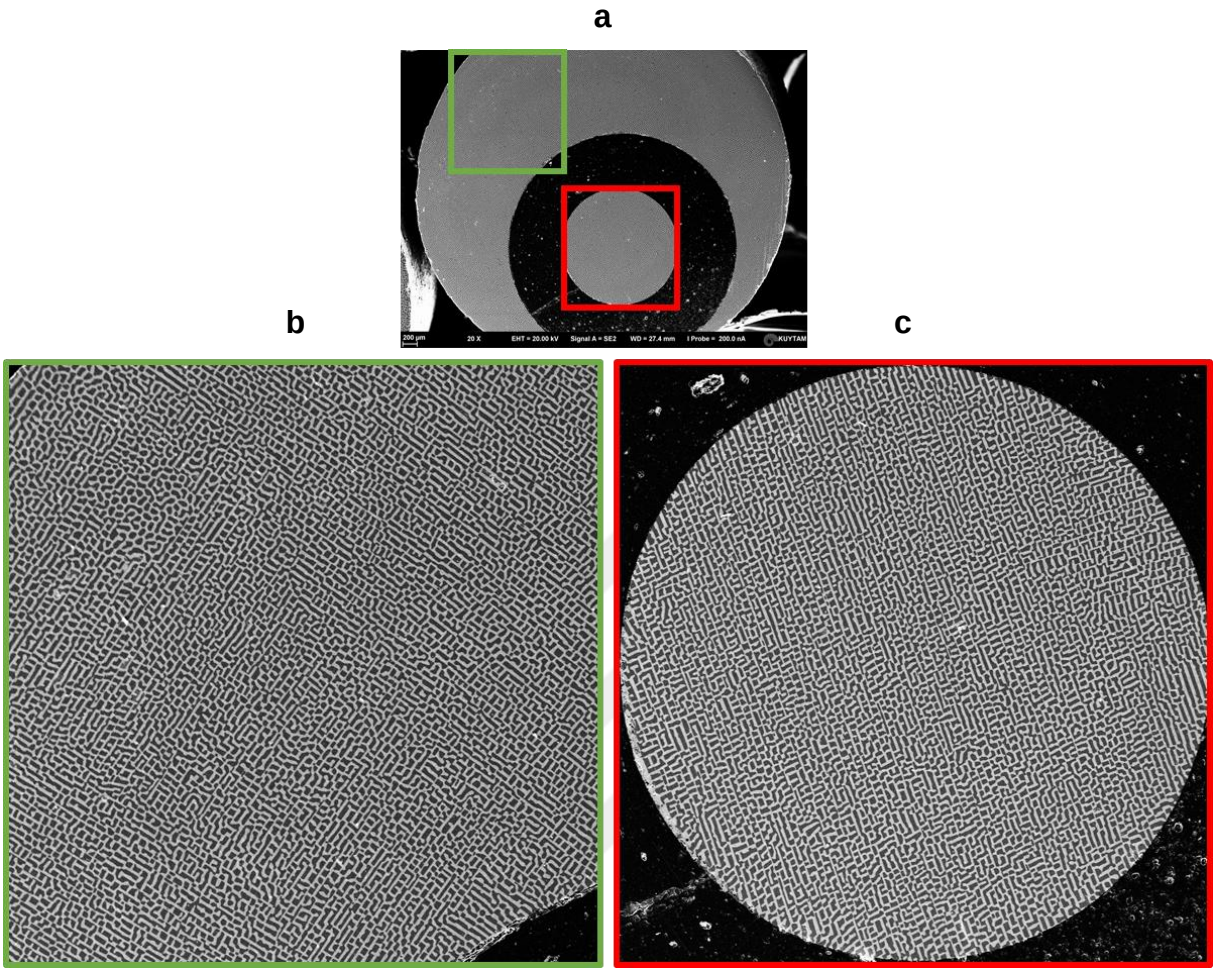

Figure 33. Initial transient microstructure obtained at samples with different inner diameters (a) SEM image of the whole sample directionally solidified with V = 0.1 μm/s at 40 mm growth length (b) The microstructure within the 5 mm diameter sample (c) The microstructure inside the 1.5 mm diameter sample.

At 60 mm growth length, mainly chain-like structure is observed both inside and outside of the alumina tube. At some regions, the microstructure is aligned in some specific directions (Figure 34).

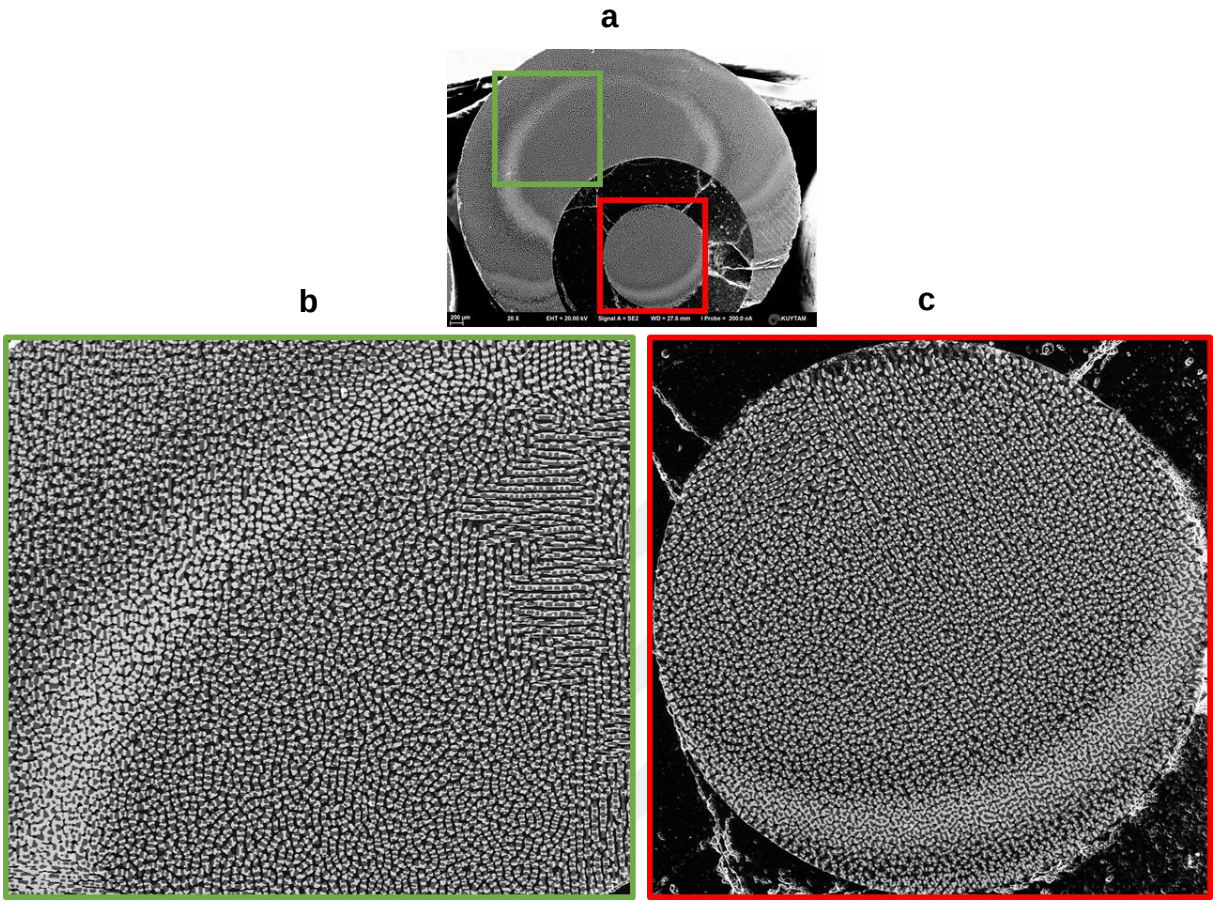

Figure 34. Mostly chain-like structure obtained at samples with different inner diameters (a) SEM image of the whole sample directionally solidified with V = 0.1 μm/s at 60 mm growth length (b) The microstructure within the 5 mm diameter sample (c) The microstructure inside the 1.5 mm diameter sample.

At 80 mm growth length, the microstructures become different inside and outside of the sleeve while chain-like structure completely transforms to faceted structure within the 5 mm diameter sample, chain-like and irregular structures coexist at the sample with 1.5 mm diameter (Figure 35). If cross-section views between 60 and 80 mm growth lengths were investigated, chain-like structure and faceted structure would have probably coexist.

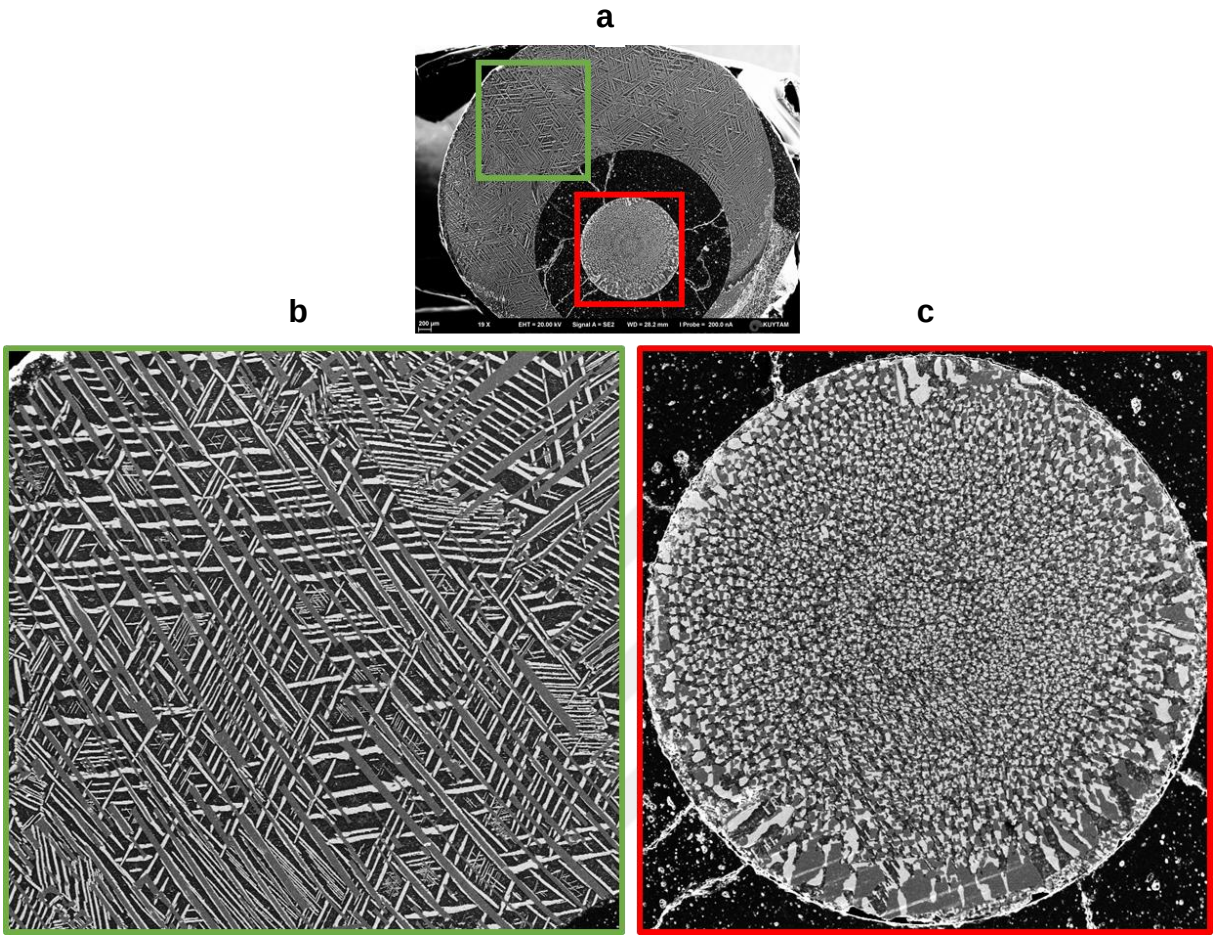

Figure 35. Faceted structure obtained in 5 mm diameter sample while structure is obtained in in 1.5 mm diameter sample after directional solidification at V = 0.1 μm/s and GL = 80 mm growth length (b) The microstructure within the 5 mm diameter sample (c) The microstructure inside the 1.5 mm diameter sample.

At 100 mm growth length, the whole microstructure within both samples is faceted. This suggests that segregation is sufficiently high to transform chain-like structure to faceted structure even in 1.5 mm diameter sample (Figure 36).

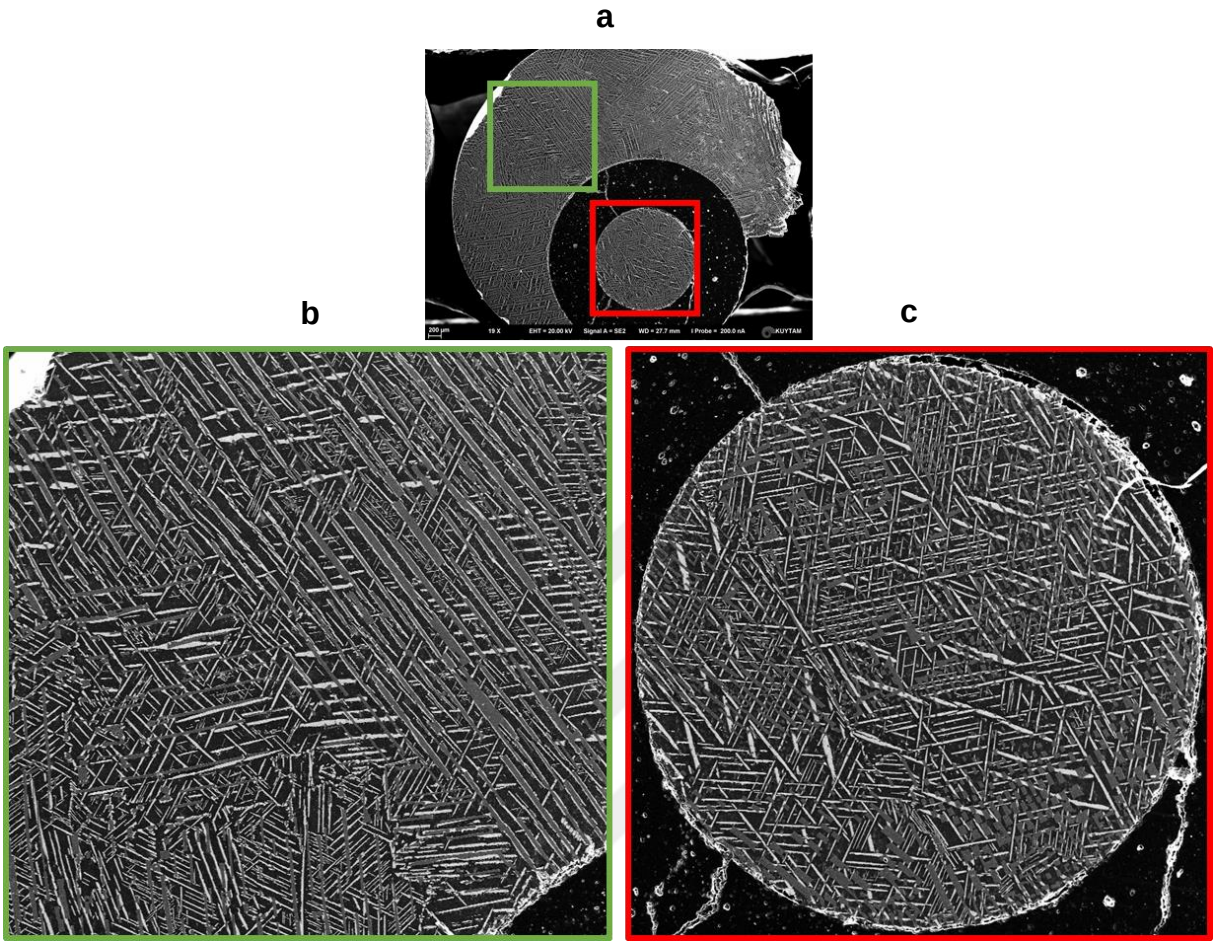

Figure 36. Faceted structure obtained at samples with different inner diameters (a) SEM image of the whole sample directionally solidified with V = 0.1 μm/s at 100 mm growth length (b) The microstructure within the 5 mm diameter sample (c) The microstructure inside the 1.5 mm diameter sample.

As a result, by the help of 1.5 mm diameter alumina tube, two samples having different cross-sectional areas are directionally solidified. The approximate specific area is 2.01 mm^2 inside the 1.5 mm diameter alumina tube and it is 15.35 mm^2 outside of it. Due to the difference in convection rates by different liquid volume, different microstructures are obtained at 80 mm growth length which shows using smaller sample diameter slows down segregation of dense elements.

3.1.6. Microstructural Characterization

The relationship between velocity and eutectic spacing at the minimum undercooling temperature is shown in Jackson-Hunt (J&H) theory as given in equation (4).

$$\lambda^2 V = \frac{K_c}{K_r} = \text{Constant} \qquad (4)$$

In order to check whether this scaling law is valid for the eutectic spacing parameters defined in this study, steady-state microstructures obtained from directional solidification experiments at different velocities are examined. Feret technique is used to determine eutectic spacing parameters which are λ_1^{α}, λ_1^{β}, and λ_2, and the results are presented in Table 5. λ_1^{α} value of Ag_2Al phase is larger than λ_1^{β} value of Al_2Cu phase because coarsening of Ag_2Al due to rejection of Ag from (Al) phase after solidification causes thicker Ag_2Al phases. Moreover, eutectic spacing measurements taken from corresponds to 3 mm and 5 mm sample are presented.

Table 5. Eutectic spacing parameters measured in samples grown with different growth velocities and with different diameters.

Velocity (μm/s)	Sample Diameter (mm)	λ_1^{α} (μm)	λ_1^{β} (μm)	λ_2 (μm)
0.1	5	49.56	46.64	22.12
0.5	5	20.38	18.61	13.81
1.0	5	12.99	11.84	7.21
1.5	5	12.10	10.16	6.37
4.0	5	8.20	6.53	4.73
1.0	3	11.62	9.55	7.42
1.5	3	10.31	8.75	6.63
4.0	3	7.58	5.14	4.29

The data shown in Table 5 is plotted in Figure 37 and Figure 38. Logarithmic scale is used to check whether the data follows scaling law of J&H. These data are fit to $y = \lambda^2 V$ equation and the y value that has the minimum R^2 errors for λ_1^α, λ_1^β, λ_2 are tabulated in Table 6.

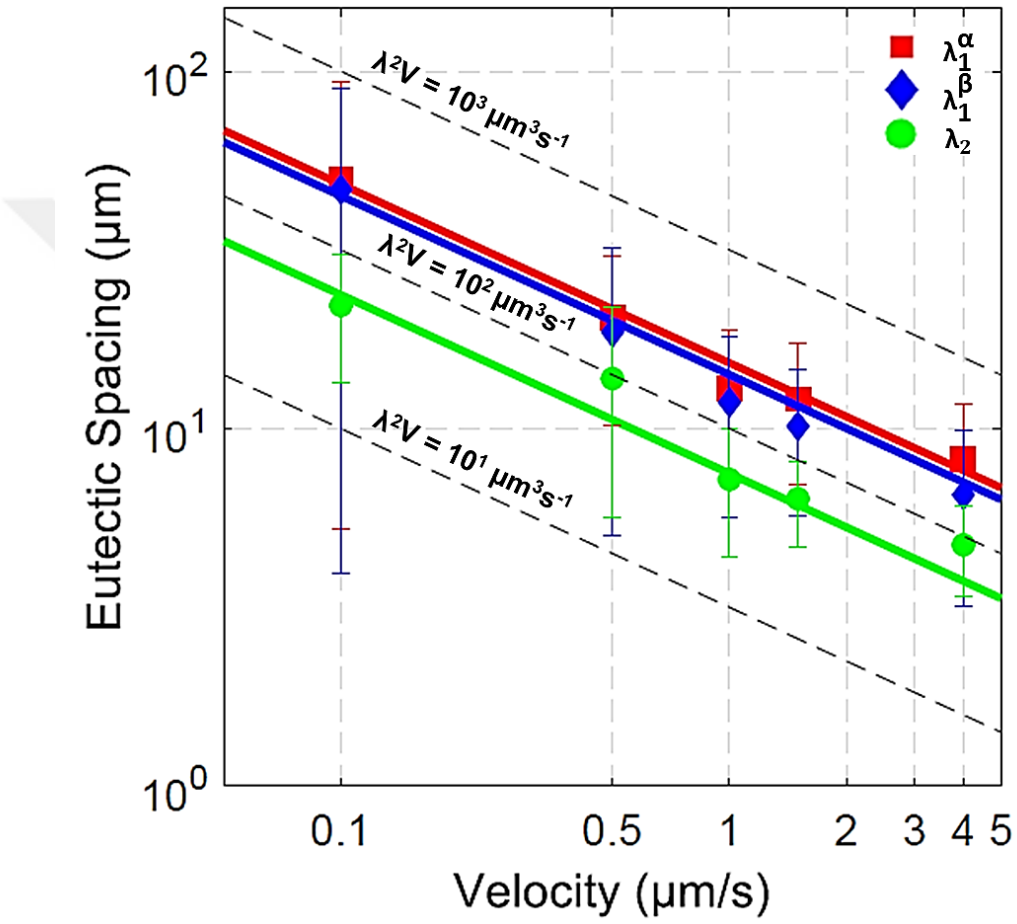

Figure 37. Eutectic spacing vs. velocity graph in logarithmic scale for 5 mm diameter samples. Fitting is applied by using $\lambda^2 V$ equation and error bars are calculated using standard deviation with 68%.

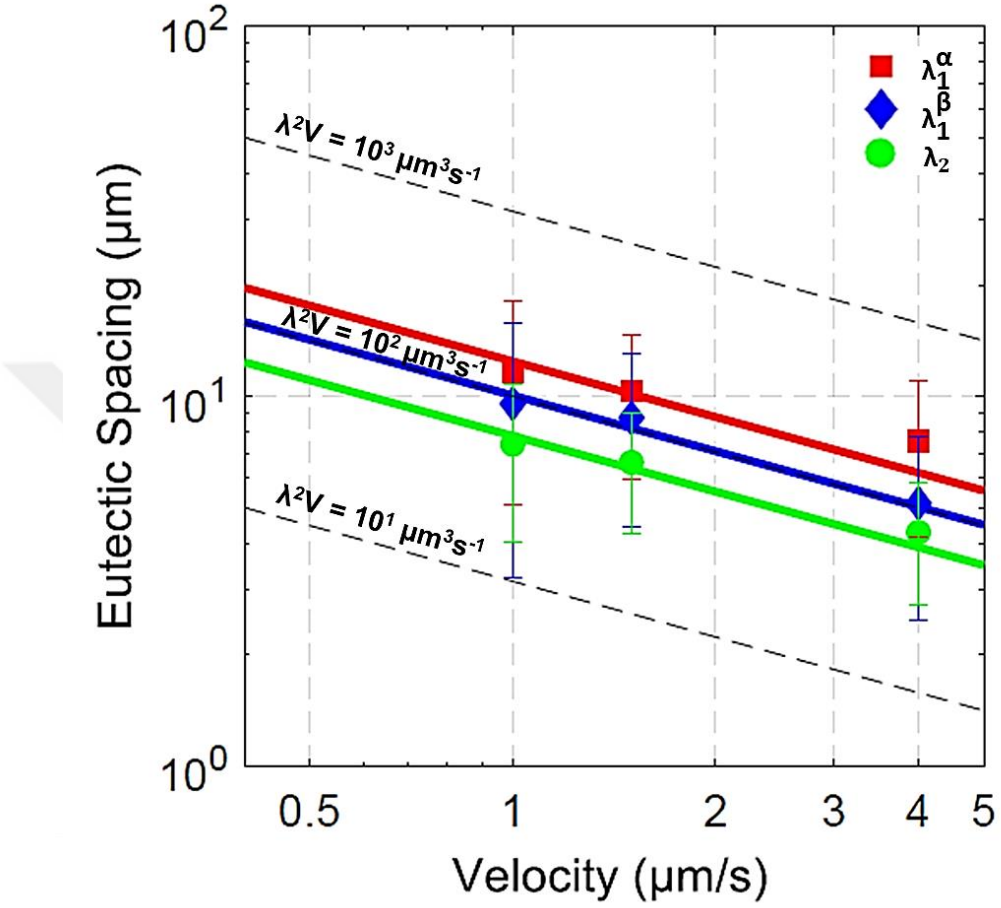

Figure 38. Eutectic spacing vs. velocity graph in logarithmic scale for 3 mm diameter samples. Fitting is applied by using λ^2V equation and error bars are calculated using standard deviation with 68%.

Table 6. Measured λ^2V for samples with 3 and 5 mm diameters.

Sample Diameter (mm)	$(\lambda_1^\alpha)^2 V$ ($\mu m^3 s^{-1}$)	$(\lambda_1^\beta)^2 V$ ($\mu m^3 s^{-1}$)	$(\lambda_2)^2 V$ ($\mu m^3 s^{-1}$)
5	233±44	201±51	56±13
3	155±49	101±23	61±11

Both eutectic spacing and $\lambda^2 V$ values are higher for 5 mm diameter sample compared to 3 mm diameter sample. Convection area is higher in higher cross-sectional area, which allows more atoms to transport. This makes thicker phase formation possible and since the thicker phase is the higher eutectic spacing, the values are high for 5 mm sample.

3.1.7. Rainbow Structure

Although chain-like structure is the mostly observed microstructure, due to shift from eutectic composition during long experiments, employed velocity ranges etc., different microstructures can be observed in Al-Ag-Cu ternary system. Paw structure and faceted structure are explained in the previous sections but there are some other structures observed in different grains or growth lengths.

Longitudinal analysis show that S/L interface is planar but due to surface tension between the walls and the sample, there is a curvature between S/L interface and the denser elements in the liquid may transport towards the walls. Although this microstructure is rarely observed there are two examples from 0.1 and 1.5 μm/s velocity experiments (Figure 39 and Figure 40). There are intense circular white bands growing from center to edge of the sample. These areas are Ag_2Al phase rich whereas around the band black phase is dominant.

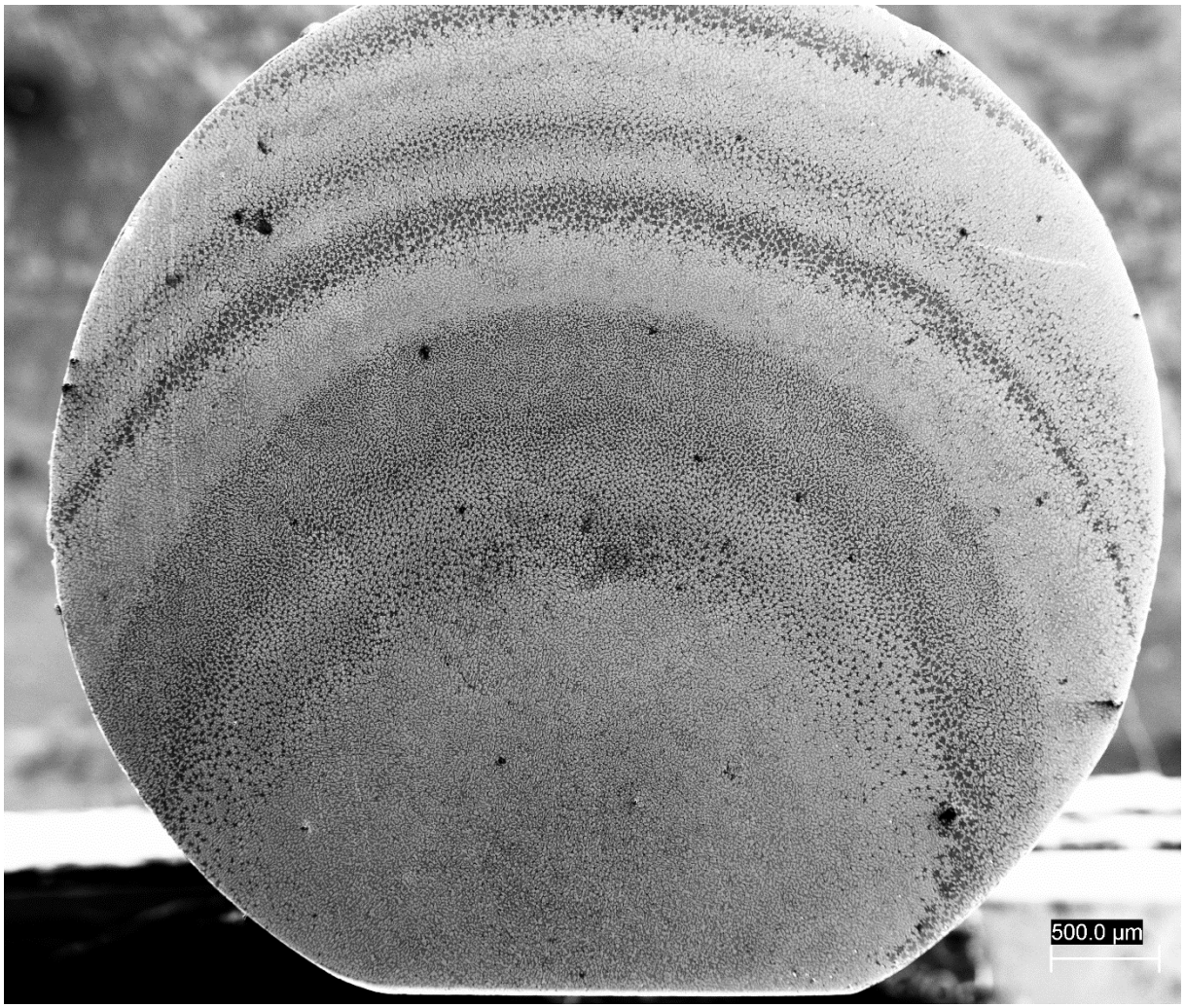

Figure 39. Rainbow structure observed in directionally solidified (V = 0.1 µm/s) sample at 20 mm growth length. Sample diameter is 5 mm.

In Figure 40, only one band is observed and the microstructure is totally different at different areas. For example, chain-like structure exists below the band while irregular structure is observed above the band. Formation of rainbow structure may indicate elemental gradient at the S/L interface, which triggers different microstructure formation.

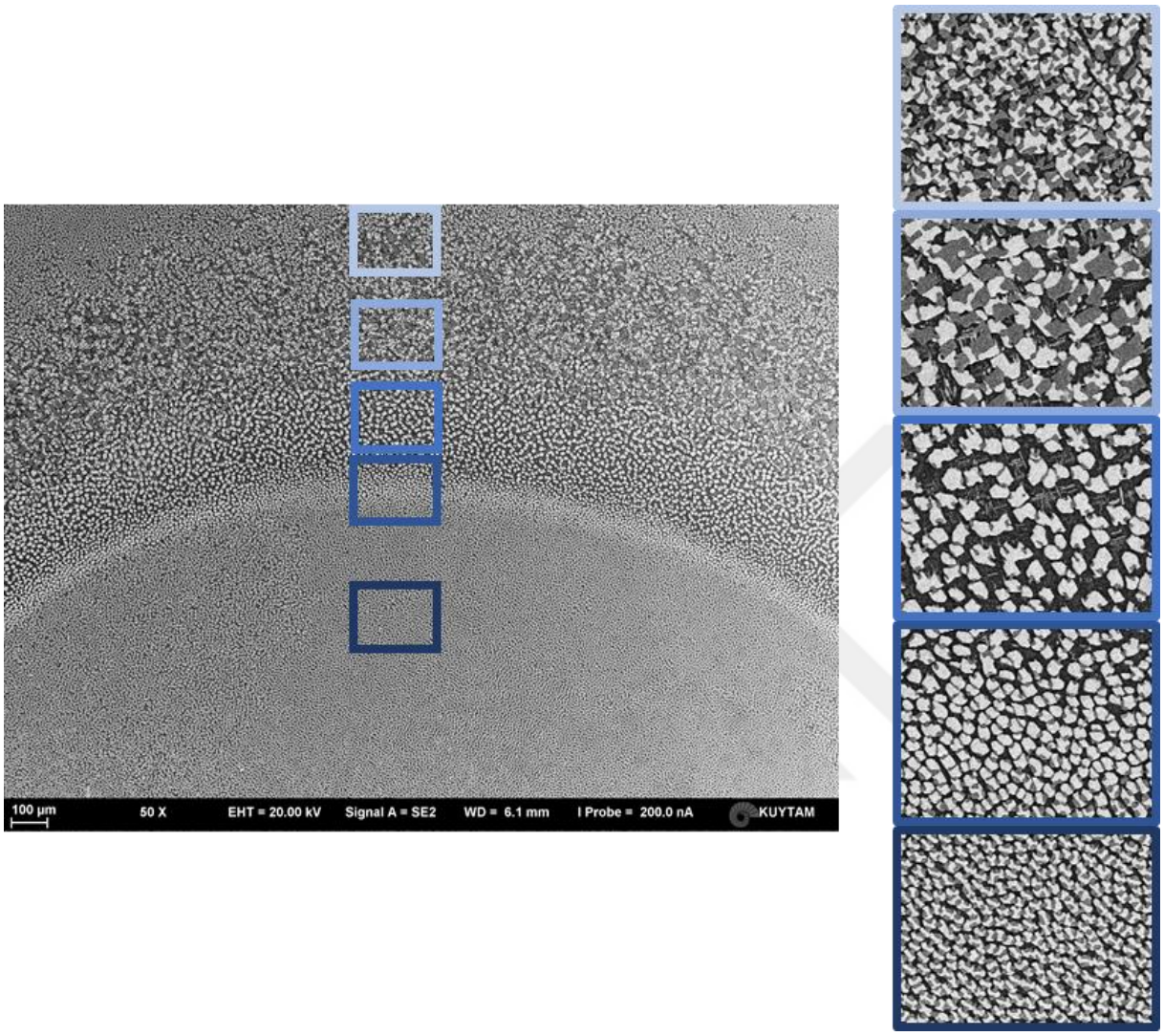

Figure 40. Rainbow structure observed in directionally solidified (V = 1.5 µm/s) sample at 80 mm growth length. Sample diameter is 3 mm.

4. SUMMARY & CONCLUSION

In this study, Al-Ag-Cu eutectic system is characterized by using Bridgman type directional solidification technique. Microstructures are analyzed by using both optical and scanning electron microscopes. Different solidification velocities, growth lengths, sample diameters are examined to investigate microstructure evolution understand the dynamics of phase arrangements. The conclusions are listed below:

- Four main microstructures which are initial transient, chain-like structure, faceted structure, and paw structure are observed at different velocity and growth length.
- The mostly observed microstructure of directionally solidified Al-Ag-Cu ternary eutectic system is chain-like structure. This structure is composed of ladder structure of alternating Ag_2Al and Al_2Cu which are aligned parallel to (Al) matrix phase.
- We established a technique to quantitatively analyze chain-like structure by implementing Feret technique and defined eutectic spacing as λ_1^{α}, λ_1^{β}, λ_2.
- Formation of paw structure is possible at velocities higher than 1.5 μm/s at minimum 60 mm growth length. This structure is composed of alternating rod-like Ag_2Al and Al_2Cu phases while (Al) phase grows parallel to them.
- Initial transient structures being composed of mainly two phases which are Ag_2Al and Al_2Cu are observed at velocities lower than 1.5 μm/s and at maximum 40 mm growth length. This is because Al concentration is insufficient to form (Al) phase until the pile up at the S/L interface.
- Faceted structure forms at velocities lower than 0.5 μm/s at minimum 80 mm growth length. ICP and DSC tests proves that elemental shift from eutectic point causes precipitation of Ag_2Al facets. Decreasing elemental shift by decreasing size of the sample delays faceted structure formation due to lower convection rate.
- Eutectic spacing values calculated by Feret technique obey the $\lambda^2 V$ rule within the stability region. By using this approach different eutectic spacing values at different velocities can be forecasted.

As the future work, micro-tomography or serial sectioning from the cross-sections can improve the quality of the data so that limits of transformations in the microstructures can be established. Although transformation from chain-like structure to paw structure is explained by changing shape of intermetallic phases, more detailed results can be obtained by micro-tomography or serial sectioning. In addition, for the investigation of the formation of different structures, crystallographic orientation relationships among the phases in chain-like structure as well as paw structure can be analyzed by using EBSD technique. It is proved that formation of faceted structure is affected by elemental shift so that microgravity experiments can improve the understanding of directional solidification in only diffusive environment by minimizing the effect of convection and segregation of denser elements. Moreover, stability regions of different phases and morphologies in ternary eutectic Al-Cu-Ag system should be found by experiments with velocity jumps associated with growth length analysis.

5. REFERENCES

1. Jackson, K.A. and J.D. Hunt, *Lamellar and rod eutectic growth.* Transactions of the Metallurgical Society of AIME, 1966. **236**(8): p. 1129.
2. Dantzing, J. and Rappaz M., *SOLIDIFICATION*. 2ND ED. ed. 2017, BOCA RATON: CRC PRESS.
3. Zhu, M.F. and C.P. Hong, *Modeling of irregular eutectic microstructures in solidification of Al-Si alloys.* Metallurgical and Materials Transactions A-Physical Metallurgy and Materials Science, 2004. **35A**(5): p. 1555-1563.
4. Wanqi, J., *Unidirectional Solidification of Al-Si Eutectic with the Accelerated Crucible Rotation Technique.* Metallurgical Transactions A, 1992. **23A**: p. 1363-1370.
5. Steen, H.A.H. and A. Hellawell, *Structure and properties of aluminum-silicon eutectic alloys.* Acta Metallurgica, 1972. **20**(3): p. 363.
6. Serefoglu, M. and R.E. Napolitano, *On the role of initial conditions in the selection of eutectic onset mechanisms in directional growth.* Acta Materialia, 2011. **59**(3): p. 1048-1057.
7. Serefoglu, M. and R.E. Napolitano, *Onset of rod eutectic morphology in directional solidification.* International Journal of Cast Metals Research, 2009. **22**(1-4): p. 228-231.
8. Serefoglu, M., et al., *Dynamics of rod eutectic growth patterns in confined geometry*, in *3rd International Conference on Advances in Solidification Processes*. 2012.
9. Serefoglu, M., *Pattern Selection Dynamics in Rod Eutectics*, in *Materials Science and Engineering*. 2009, Iowa State University: Ames, Iowa. p. 188.
10. Napolitano, R.E., C. Jung, and H. Meco, *Growth mechanisms in low-velocity Al-Si eutectics*, in *Solidification Processes and Microstructures: A symposium in Honor of W. Kurz*, M. Rappaz, Editor. 2004, The Minerals, Metals, and Materials Society: Charlotte, N.C. p. 245-250.
11. Karma, A., et al., *Overstability of Lamellar Eutectic Growth below the Minimum-Undercooling Spacing.* Metallurgical and Materials Transactions A, 2004. **35 A**: p. 1815-1828.
12. Akamatsu, S., et al., *Real-time study of thin and bulk eutectic growth in succinonitrile-(d)camphor alloys.* Journal of Crystal Growth, 2007. **299**(2): p. 418.
13. Sturz, L., et al., *Organic alloy systems suitable for the investigation of regular binary and ternary eutectic growth.* Journal of Crystal Growth, 2004. **270**: p. 273-282.

14. Witusiewicz, V.T., et al., *Phase equilibria and eutectic growth in quaternary organic alloys amino-methyl-propanediol-(D)camphor-neopentylglycol-succinonitrile (AMPD-DC-NPG-SCN).* Journal of Crystal Growth, 2006. **297**(1): p. 117-132.
15. Witusiewicz, V.T., et al., *In situ observation of microstructure evolution in low-melting Bi-In-Sn alloys by light microscopy.* Acta Materialia, 2005. **53**(13): p. 3663-3669.
16. Rex, S., et al., *Transient eutectic solidification in In-Bi-Sn: Two-dimensional experiments and numerical simulation.* Materials Science and Engineering A-Structural Materials Properties Microstructure and Processing, 2005. **413**: p. 249-254.
17. Bottin-Rousseau, S., S. Akamatsu, and G. Faivre, *Dynamical polygonization below the cellular-bifurcation threshold in thin-sample directional solidification.* Physical Review B, 2002. **66**(5).
18. Bottin-Rousseau, S., et al., *Stability of three-phase ternary-eutectic growth patterns in thin sample.* Acta Materialia, 2016. **109**: p. 259-266.
19. Akamatsu, S., S. Moulinet, and G. Faivre, *The Formation of Lamellar-Eutectic Grains in Thin Samples.* Metallurgical And Materials Transactions A, 2001. **32A**: p. 2039-2048.
20. Akamatsu, S., et al., *A theory of thin lamellar eutectic growth with anisotropic interphase boundaries.* Acta Materialia, 2012. **60**(6-7): p. 3199-3205.
21. Mohagheghi, S. and M. Şerefoğlu, *Quasi-isotropic and locked grain growth dynamics in a three-phase eutectic system.* Acta Materialia, 2018. **151**: p. 432-442.
22. Mccartney, D.G., R.M. Jordan, and J.D. Hunt, *The Structures Expected in a Simple Ternary Eutectic System .2. The Al-Ag-Cu Ternary-System.* Metallurgical Transactions a-Physical Metallurgy and Materials Science, 1980. **11**(8): p. 1251-1257.
23. Wilde De, J., L. Froyen, and S. Rex, *Coupled two-phase [a(Al)+h(Al2Cu)] planar growth and destabilisation along the univariant eutectic reaction in Al–Cu–Ag alloys.* Scripta Materialia, 2004. **51**: p. 533-538.
24. Wilde De, J. and L. Froyen, *Microstructures Observed During Directional SOlidification Along The Univariant Eutectuc Reaction In A Ternary Al-Cul-Si Alloy.* Materials Science Forum, 2006. **508**: p. 51-56.
25. Hecht, U., et al., *Eutectic solidification of ternary Al-Cu-Ag alloys: Coupled growth of alpha(Al) and Al2Cu in univariant reaction*, in *Solidification And Gravity Iv*. 2006. p. 57-62.
26. Hecht, U., et al., *Coupled growth of Al-Al2Cu eutectics in Al-Cu-Ag alloys*, in *3rd International Conference on Advances in Solidification Processes*. 2012, IOP Publishing Ltd: Bristol.

27. De Wilde, J., et al., *Two-phase planar and regular lamellar coupled growth along the univariant eutectic reaction in ternary alloys: An analytical approach and application to the Al-Cu-Ag system.* Journal of Applied Physics, 2005. **97**(11): p. 9.
28. Dennstedt, A. and L. Ratke, *Microstructures of Directionally Solidified Al-Ag-Cu Ternary Eutectics.* Transactions of the Indian Institute of Metals, 2012. **65**(6): p. 777-782.
29. Genau, A. and L. Ratke, *Morphological characterization of the Al-Ag-Cu ternary eutectic.* International Journal of Materials Research, 2012. **103**(4): p. 469-475.
30. Choudhury, A., *Pattern-Formation During Self-organization in Three-Phase Eutectic Solidification.* Transactions of the Indian Institute of Metals, 2015. **68**(6): p. 1137-1143.
31. Steinmetz, P., et al., *Phase-field study of the pattern formation in Al–Ag–Cu under the influence of the melt concentration.* Computational Materials Science, 2016. **121**: p. 6-13.
32. Hotzer, J., et al., *Influence of growth velocity variations on the pattern formation during the directional solidification of ternary eutectic Al-Ag-Cu.* Acta Materialia, 2017. **136**: p. 335-346.
33. Himemiya, T. and T. Umeda, *Three-Phase Planar Eutectic Growth Models for a Ternary Eutectic System.* Materials Transactions, 1999. **40**(7): p. 665-674.
34. Sargin, I., *Invariant and univariant eutectic solidification in ternary alloys*. 2015, Iowa State University Digital Repository.
35. Witusiewicz, V.T., et al., *The Ag–Al–Cu system: Part I: Reassessment of the constituent binaries on the basis of new experimental data.* Journal of Alloys and Compounds, 2004. **385**(1–2): p. 133-143.
36. Okamoto, H., M.E. Schlesinger, and E.M. Mueller, *ASM Handbook : Alloy Phase Diagrams, Volume 3*. 2016, ASM International.
37. Kurz, W. and D.J. Fisher, *Fundamentals of solidification*. 4th rev. ed. ed. 2005, Switzerland: Trans Tech Publications.
38. Witusiewicz, V.T., et al., *The Ag–Al–Cu system: II. A thermodynamic evaluation of the ternary system.* Journal of Alloys and Compounds, 2005. **387**(1–2): p. 217-227.
39. Callister, W.D., *Material science and engineering : an introduction. 7th ed*. 2006: Wiley.